HEALTH AND MEDICINE

The clinical antiprotozoal drug halofuginone promotes weight loss by elevating GDF15 and FGF21

Suowen Xu[1,2,3,4]*†, Zhenghong Liu[1]†, Tian Tian[1]†, Wenqi Zhao[1]†, Zhihua Wang[1], Monan Liu[1], Mengyun Xu[1], Fanshun Zhang[1], Zhidan Zhang[1], Meijie Chen[1], Yanjun Yin[1], Meiming Su[1], Wenxiang Fang[5], Wenhao Pan[6], Shiyong Liu[6], Min-dian Li[7], Peter J. Little[8], Danielle Kamato[9], Songyang Zhang[10], Dongdong Wang[11], Stefan Offermanns[3], John R. Speakman[12,13]*, Jianping Weng[1,2,4,14]*

Obesity is a debilitating global pandemic with a huge cost on health care due to it being a major underlying risk factor for several diseases. Therefore, there is an unmet medical need for pharmacological interventions to curb obesity. Here, we report that halofuginone, a Food and Drug Administration–approved anti-scleroderma and antiprotozoal drug, is a promising anti-obesity agent in preclinical mouse and pig models. Halofuginone suppressed food intake, increased energy expenditure, and resulted in weight loss in diet-induced obese mice while also alleviating insulin resistance and hepatic steatosis. Using molecular and pharmacological tools with transcriptomics, we identified that halofuginone increases fibroblast growth factor 21 (FGF21) and growth differentiation factor 15 (GDF15) levels via activating integrated stress response. Using *Gdf15* and *Fgf21* knockout mice, we show that both hormones are necessary to elicit anti-obesity changes. Together, our study reports the beneficial metabolic effects of halofuginone and underscores its utility in treating obesity and its associated metabolic complications, which merits clinical assessment.

INTRODUCTION

Obesity, characterized by the pathological and ectopic accumulation of adipose tissue due to relative overnutrition, is widely acknowledged as a chronic degenerative condition that predisposes individuals to various metabolic-related disorders, including cardiovascular disease, type 2 diabetes mellitus, metabolic dysfunction–associated steatotic liver disease, and cancer (*1*–*3*). Obesity constitutes one of the greatest health care challenges and imposes a heavy economic burden on public health systems because of its rising prevalence (*4*, *5*). Efforts to manage obesity through lifestyle interventions (including dietary changes and physical activity) and early therapeutic interventions have achieved limited success. Bariatric surgery is successful in achieving weight loss and decreasing obesity; however, it is associated with risks, making it not feasible for treatment of a large population. Consequently, the development of previously unidentified therapeutic agents and strategies is deemed a more effective approach for sustained obesity management at the population level (*6*, *7*). This is exemplified by the recent success of glucagon-like peptide-1 receptor (GLP1R) agonists (*8*, *9*). However, in a portion of the treated population, these drugs cause undesirable side effects (*10*), underscoring the need to continuously find and develop innovative drugs acting via novel pathways.

Restriction of dietary protein or certain amino acids, such as methionine and branched-chain amino acids, promotes metabolic health through pathways including GCN2 (general control nonderepressible 2)/ATF4 (activating transcription factor 4), mechanistic target of rapamycin kinase, and adenosine monophosphate–activated protein kinase (*11*–*13*). Halofuginone (HF), a derivative of febrifugine from antimalarial Chinese herbal medicine Changshan, is a Food and Drug Administration–approved, orally bioavailable drug used to treat scleroderma and protozoal infections (*14*). HF functions by binding to and inhibiting aminoacyl-tRNA synthetases, with a primary action on glutamyl-prolyl-tRNA synthetase (EPRS) (*15*). This inhibition leads to activation of the amino acid starvation (AAS) response pathway and integrated stress response (ISR) signaling. Inhibition of EPRS by HF leads to the accumulation of uncharged tRNAs, initiating autophosphorylation of the amino acid sensor GCN2, resulting in phosphorylation of eIF2α and increased expression of ATF4 (*14*). HF demonstrates a broad therapeutic potential against various medical conditions through its anti-inflammatory, anti-fibrotic, and antitumor effects (*14*, *16*–*18*). However, it remains largely unclear whether HF exerts metabolic benefits by treating obesity-associated metabolic disorders.

In this study, we report HF as a potential drug to treat obesity by elevating growth differentiation factor 15 (GDF15) and fibroblast growth factor 21 (FGF21) via ISR pathway, which respectively

[1]Department of Endocrinology, Centre for Leading Medicine and Advanced Technologies of IHM, The First Affiliated Hospital of USTC, Division of Life Sciences and Medicine, University of Science and Technology of China, Hefei 230001, China. [2]Anhui Provincial Key Laboratory of Metabolic Health and Panvascular Diseases, Hefei 230001, China. [3]Department of Pharmacology, Max Planck Institute for Heart and Lung Research, Bad Nauheim 61231, Germany. [4]Institute of Endocrine and Metabolic Diseases, University of Science and Technology of China, Hefei 230001, China. [5]The First Affiliated Hospital of USTC, Division of Life Sciences and Medicine, University of Science and Technology of China, Hefei 230001, China. [6]Laboratory of Precision and Intelligent Chemistry, Department of Polymer Science and Engineering, University of Science and Technology of China, Hefei 230026, China. [7]Department of Cardiovascular Medicine, Center for Circadian Metabolism and Cardiovascular Disease, MOE Key Laboratory of Geriatric Cardiovascular and Cerebrovascular Disease, Southwest Hospital, Army Medical University, Chongqing, China. [8]Department of Pharmacy, Guangzhou Xinhua University, No. 721, Guangshan Road 1, Guangzhou 510520, China. [9]Institute for Biomedicine and Glycomics, Griffith University, Nathan, Queensland 4111, Australia. [10]Toronto General Hospital Research Institute, University Health Network, Toronto, Ontario, Canada. [11]Centre for Metabolism, Obesity, and Diabetes Research, McMaster University, Hamilton, Ontario, Canada. [12]Shenzhen Key Laboratory of Metabolic Health, Center for Energy Metabolism and Reproduction, Shenzhen Institutes of Advanced Technology, Chinese Academy of Sciences, Shenzhen 518055, China. [13]School of Biological Sciences, University of Aberdeen, Aberdeen AB24 3FX, UK. [14]Department of Endocrinology, The First Affiliated Hospital of Anhui Medical University, Hefei 230022, China.
*Corresponding author. Email: wengjp@ustc.edu.cn (J.W.); j.speakman@abdn.ac.uk (J.R.S.); sxu1984@ustc.edu.cn (S.X.)
†These authors contributed equally to this work.

inhibit energy intake and increase energy expenditure, thus promoting weight loss in obese animal models. Our findings support the potential to repurpose antiprotozoal drug HF for treating obesity and its metabolic complications.

RESULTS

HF promotes weight loss in obese animal models

Taking into consideration relevant preclinical and clinical dosing regimens (*19*, *20*), we investigated the tissue distribution and pharmacokinetics of HF in normal mice. We chose intravenous and oral administration to assess the drug bioavailability. HF was administered intravenously (168 μg/kg) or orally (840 μg/kg), and HF concentration was measured in blood and organs. After intravenous injection, HF was detected in the heart plasma, portal plasma, heart, liver, spleen, lung, kidney, fat, and muscle. The drug concentration peaked at 15 min postinjection (fig. S1A). When given orally, HF mainly accumulated in the stomach and intestines (fig. S1B). The oral bioavailability of HF was 60.3%. Two hours after oral administration, HF reached its peak plasma concentration (12.5 ± 2.9 ng/ml). The half-life of orally and intravenously administered HF was around 5.0 and 3.4 hours, respectively (fig. S1C). Considering that intravenous injection, while having high bioavailability, is technically challenging, we primarily used intraperitoneal injection of HF in subsequent experiments to evaluate its effects.

In clinical trials, for chronic administration of HF, oral dosing at 0.5 mg/day is recommended (*19*, *21*). After dosage conversion between human and mice and consideration of oral bioavailability (*22*), we have selected 100 μg/kg to evaluate the safety profile of HF in normal chow diet–fed C57BL/6J mice (fig. S2A). We observed that long-term administration of HF reduced weight gain rate in lean mice (fig. S2B). A subsequent comprehensive comparison of blood cell counts, histopathology, organ weights, and serum parameters indicative of injury in the liver, heart and kidney function between HF and vehicle suggests no noticeable toxicity of HF in normal male C57BL/6J mice (fig. S2, C to R).

To assess the potential therapeutic benefits of HF in reducing obesity, we treated diet-induced obese (DIO) mice with escalating doses (25, 50, 100 μg/kg) of HF and liraglutide (200 μg/kg) (a reference drug, a GLP1R agonist) every 2 days for 8 weeks while continuing high-fat diet (HFD) feeding (Fig. 1, A and B). In the highest dosage group of HF treatment (100 μg/kg), the body weight of mice decreased by 22.3% compared to the vehicle group, whereas the positive control drug, liraglutide, resulted in a 15.96% reduction in body weight (Fig. 1C). The HF (25 and 50 μg/kg)–treated groups also exhibited significant weight-lowering effects. Assessment of lean and fat mass percentage show that HF-treated mice exhibited a reduction in total fat mass without affecting lean mass percentage (Fig. 1D). Consistently, HF (100 μg/kg) significantly reduced serum levels of triglycerides (TG) and total cholesterol (TC) (fig. S3, A and B). In addition, obese mice treated with either HF or liraglutide exhibited reduced levels of alanine aminotransferase (ALT) and aspartate aminotransferase (AST) (fig. S3, C and D). There was no effect of HF on creatinine (CREA) and urea levels (fig. S3, E to F). Moreover, HF treatment was associated with a decrease in homeostatic model assessment of insulin resistance and improvements in glucose tolerance and insulin sensitivity (fig. S3, G to J). We next asked whether or not EPRS inhibition by HF is essential for the weight loss effects of HF, by intraperitoneal injection of DIO mice with MAZ1310, an inactive HF derivative (unable to bind EPRS) (Fig. 1E) (*15*). Through in vitro translation experiments using rabbit reticulocyte lysate, we demonstrate that HF, but not MAZ1310, inhibits translation, and HF-mediated translation inhibition effect can be reversed by the addition of excess proline (Fig. 1F). We used MAZ1310 as a negative control in mouse dosing experiments. Compared to an equivalent dose of HF (100 μg/kg), MAZ1310 did not cause body weight loss (Fig. 1G).

HF-treated mice regained some of their lost body weight after discontinuation of the treatment (Fig. 1H). The mice in the HF-withdrawal group had less body weight (compared with vehicle) but gained about 10% body weight over a period of 4 weeks. The benefits of HF on reducing body weight also pertained to female DIO mice, which exhibited reduced body weight and enhanced insulin sensitivity (fig. S3, K and L). In the oral HF experiment, the weight loss achieved with HF at 100 μg/kg (−9.8%) was comparable to that observed with orlistat at 20 mg/kg (−8.2%). However, HF at 200 μg/kg (−27.9%) demonstrated a significantly enhanced weight loss effect (fig. S3M). HF also reduced the rate of weight gain in DIO mice housed under thermoneutral (TN) conditions (−18.8%) and *ob*/*ob* mice (−11.2%) (Fig. 1, I to J). The anti-obesity effect of HF was also extended to a swine model of obesity (Fig. 1K). These data suggest that HF promotes weight loss in different animal models.

HF suppresses food intake and increases energy expenditure

HF (100 μg/kg) administration also inhibited cumulative food intake, as well as food intake in fast-refeeding experiment (Fig. 2, A and B). The decline in the body weight was greater following HF treatment than that in pair-fed in mice (Fig. 2C). This suggests that the impact of HF was due to a combination of inhibited food intake and elevated energy expenditure. Moreover, HF treatment led to improvements in thermogenic capability, as shown by sustained elevated core temperature during cold challenge (Fig. 2D). Of note, protein analysis showed that UCP1 was up-regulated in interscapular brown adipose tissue (iBAT) of HF-treated obese mice versus vehicle (Fig. 2E). Energy expenditure of DIO mice treated with vehicle or HF also supported the findings (Fig. 2F). HF exhibited significant impacts on food intake and prompted the utilization of fat as the primary energy source as revealed by respiratory exchange ratio (RER) analysis (Fig. 2G). However, in mice fed normal chow diet, there was no effect on energy expenditure ($P > 0.05$) despite the fact that food intake was notably suppressed (fig. S4, A to C). Collectively, these findings demonstrate that HF ameliorates obesity-related phenotypes, suppresses food intake, and enhances energy expenditure in obese mice.

HF-treated mice also reduced weights of inguinal white adipose tissue (iWAT) (−35.6%) and epididymal WAT (eWAT) (−45.7%), accompanied by consistently smaller adipocyte size and diminished adipose depots (Fig. 2H and fig. S4, D and E). Compared to the vehicle group, iBAT weight was decreased in HF-treated obese mice, but the iBAT had less lipid accumulation (Fig. 2H and fig. S4F). In addition, HF reduced liver weight and ameliorated hepatic steatosis as measured by hepatic TG and TC levels and histological examination, suggesting that HF ameliorated obesity-related fatty liver (Fig. 2H and fig. S4, G to I).

HF elevates the expression of GDF15 and FGF21

To unravel the potential molecular mechanisms by which HF suppressed food intake and elevated energy expenditure and to identify common or synergistic pathways in liver and adipose tissues, we performed bulk RNA sequencing (RNA-seq) on WAT and liver of vehicle- and HF-treated

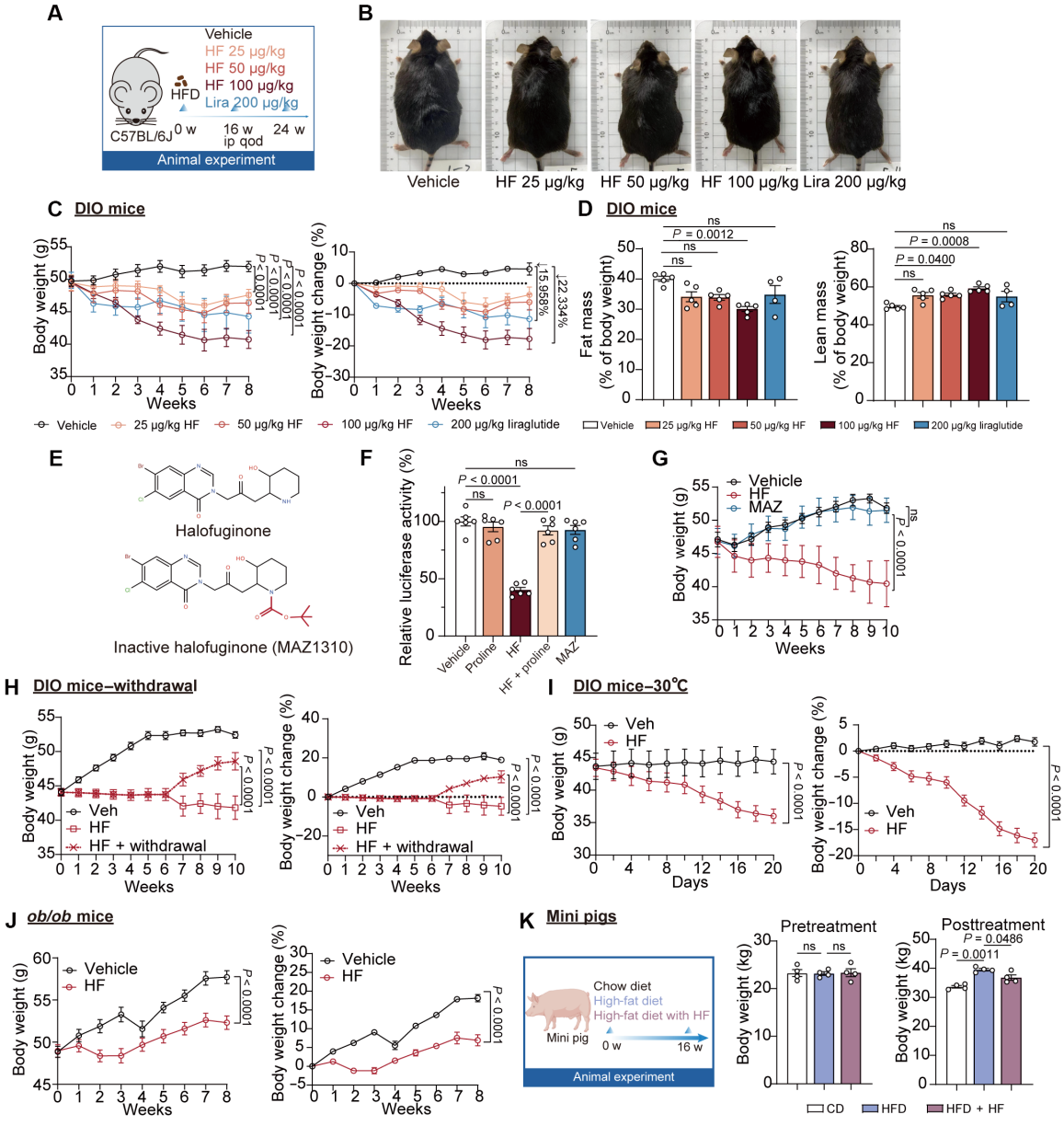

Fig. 1. HF promotes weight loss in obese animal models. (**A** to **D**) Male C57BL/6J mice were fed an HFD for 16 weeks (w) and then randomly assigned to five groups: (i) vehicle group; (ii) 25 μg/kg, (iii) 50 μg/kg, and (iv) 100 μg/kg HF treatment group; and (v) 200 μg/kg liraglutide treatment group. The mice were treated with intraperitoneal (ip) injections of vehicle or indicated drugs every 2 days. (A) Schematic diagram of study design. (B) Representative gross images of mice. (C) Body weight and % body weight change (vehicle or HF group, $n = 5$; liraglutide group, $n = 4$). (D) Fat mass and lean mass (% of body weight) by nuclear magnetic resonance scans (vehicle or HF group, $n = 5$; liraglutide group, $n = 4$). ns, not significant. (**E**) Chemical structure of HF and MAZ1310 (EPRS1 inactive compound). (**F**) Luciferase mRNA was incubated with rabbit reticulocyte lysate (RRL), and the translation process was measured using a luminescence assay (HF, 200 nM; proline, 8 mM; MAZ1310, 200 nM). (**G**) Body weight of DIO mice during vehicle, HF treatment (100 μg/kg), or MAZ treatment (100 μg/kg) (vehicle or MAZ group, $n = 5$; HF group, $n = 4$). (**H**) Body weight and % body weight change of DIO mice during vehicle, HF treatment or HF withdrawal treatment ($n = 10$). (**I**) Body weight and % body weight change of DIO mice in a TN environment (30°C) during 20 days of HF treatment (100 μg/kg, $n = 8$). (**J**) Body weight and % body weight change of *ob/ob* mice during vehicle or HF treatment (vehicle group, $n = 7$; HF group, $n = 8$, 100 μg/kg). (**K**) Body weight of obese minipigs before HF treatment and after 16-week HF treatment ($n = 4$). Data in (D) were analyzed by one-way analysis of variance (ANOVA) followed by Bonferroni's multiple comparisons test. Data in (C), (F) to (H), and (K) were determined through two-way ANOVA followed by Bonferroni's multiple comparisons test. Data in (I) and (J) were determined through two-way ANOVA.

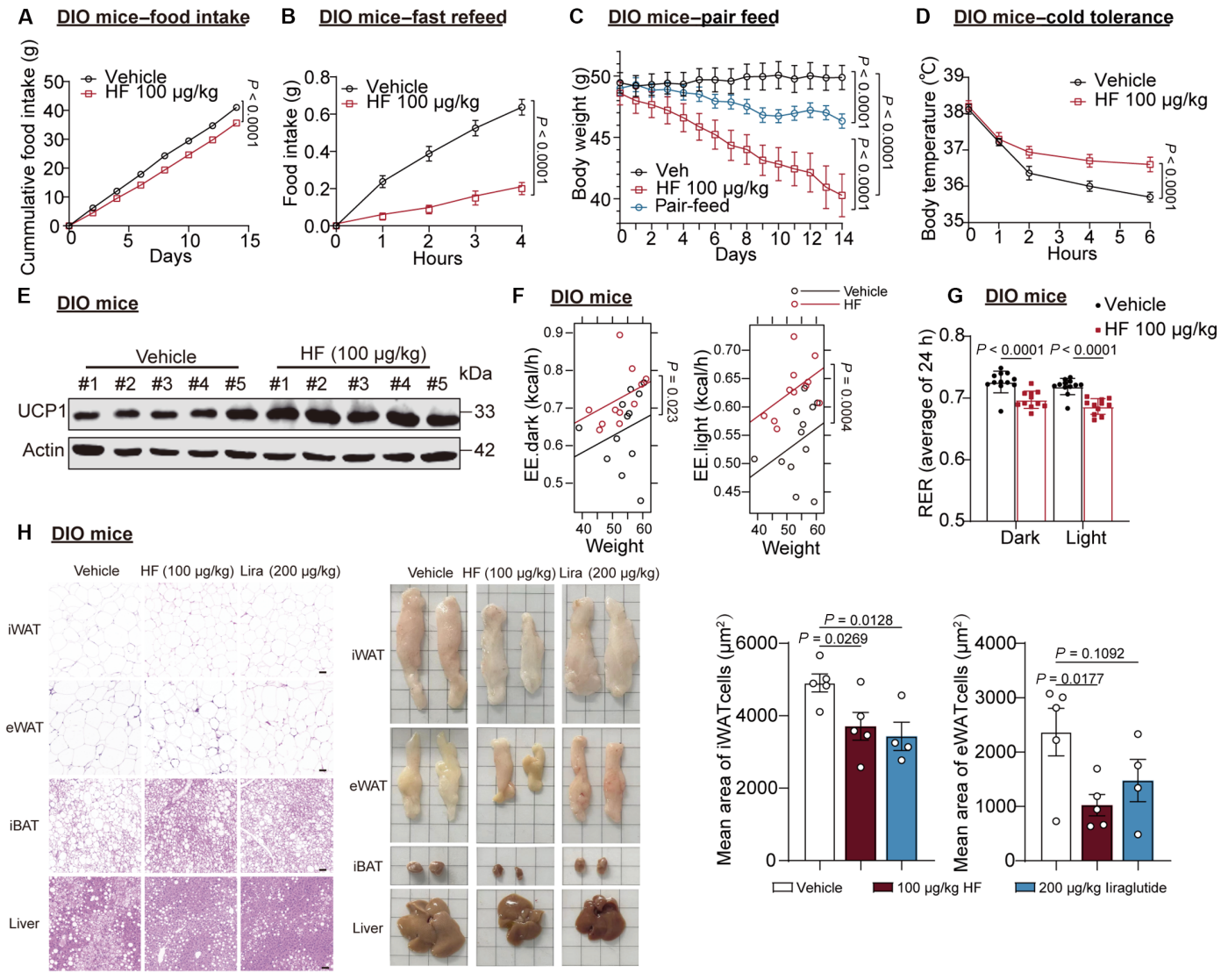

Fig. 2. HF suppresses food intake and increases energy expenditure. (**A**) Cumulative food intake of DIO mice (single cage) treated with vehicle or HF (100 μg/kg) ($n = 8$). (**B**) Food intake after fast-refeed DIO mice treated with vehicle or HF (100 μg/kg) ($n = 8$). (**C**) Changes in body weight during pair-feeding ($n = 8$). (**D**) Cold tolerance of DIO mice treated with vehicle or HF (100 μg/kg) ($n = 5$ to 6). (**E**) UCP1 protein abundance in iBAT of vehicle- or HF (100 μg/kg)–treated DIO mice ($n = 5$). (**F**) Energy expenditure (EE) in DIO mice treated with vehicle or HF (100 μg/kg) (vehicle group, $n = 12$; HF group, $n = 11$). (**G**) Average 24 hours (h) RER in DIO mice treated with vehicle or HF (100 μg/kg) (vehicle group, $n = 12$; HF group, $n = 11$). (**H**) Representative images of hematoxylin and eosin staining of adipose tissues and liver, and the quantification of adipocyte size of eWAT and iWAT (vehicle or HF group, $n = 5$; liraglutide group, $n = 4$). Scale bar, 50 μm. Data are presented as means ± SEM. Data in (A), (B), and (D) were determined through two-way ANOVA. Data in (C) were determined through two-way ANOVA by Bonferroni's multiple comparisons test. Data in (F) were determined through ANCOVA using body mass as a covariate. Bar graphs in (G) analyzed by two-way ANOVA followed by Bonferroni's multiple comparisons test. Data in (H) analyzed by one-way ANOVA followed by Fisher's least significant difference test.

DIO mice (Fig. 3, A to C). We intersected the differentially expressed genes in WAT and liver, identifying 55 genes with commonly up-regulated expression and 75 genes with commonly down-regulated expression (Fig. 3D). The livers from HF-treated mice exhibited higher expression of diverse transcripts related to the ISR, including those encoding transcription factors (*Nupr1*, *Atf4*, and *Atf5*), hepatic metabokines (*Gdf15* and *Fgf21*), and proteins involved in single-carbon (1C) metabolism (*Mthfd2*) (Fig. 3E). Consistent with previous reports in other tissues (*23*), we observed that HF activated the GCN2/ATF4 signaling pathway in mouse liver (Fig. 3F). In earlier reports, ATF4 has been identified as a transcription factor that responds to ISR and is capable of enhancing the expression of GDF15 and FGF21 (*24*–*27*). GDF15 and FGF21, in turn, participate in the regulation of energy balance through respective mechanisms of action. On the basis of previous research findings and our sequencing results, we focused on two up-regulated hormones, GDF15 and FGF21, hypothesizing that both play key roles in the weight loss effects induced by HF. Given that both FGF21 and GDF15 function as secretory proteins, there is ongoing debate regarding the primary organs/tissues that secrete GDF15, with the liver, ileum, and kidney believed to be the main sources (*24*, *25*, *28*). FGF21, on the other hand, is reported to be predominantly secreted by the

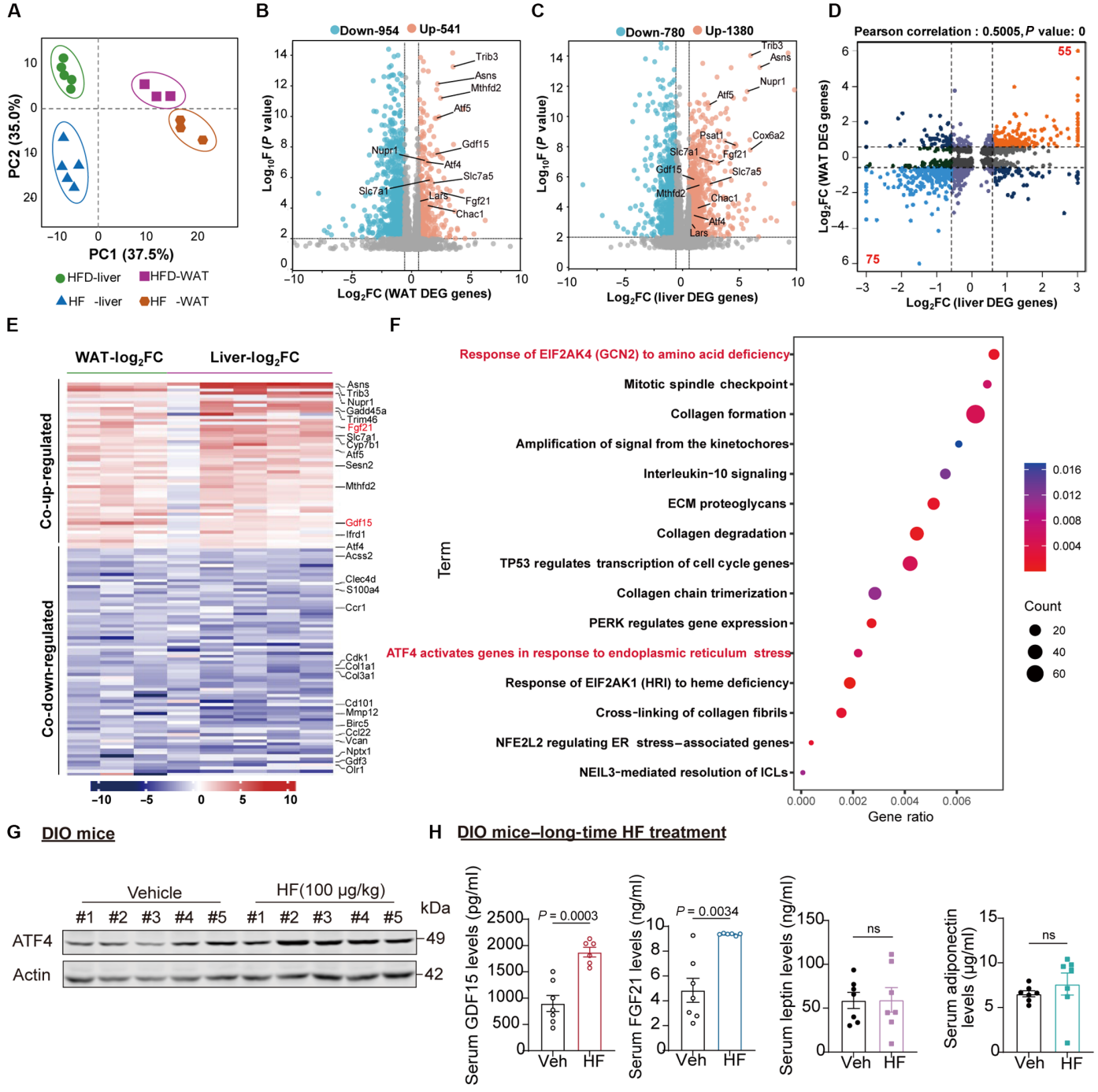

Fig. 3. HF induces the up-regulation of GDF15 and FGF21. (**A**) Principal components analysis from RNA-seq of vehicle- or HF (100 μg/kg)–treated mouse liver and WAT tissues (WAT, $n = 3$; liver, $n = 5$). (**B**) Volcano plot of significantly down-regulated (blue) and up-regulated (red) genes in WAT from mice as described in (A) ($|Log_2FC| > 1.5$, P value <0.01). (**C**) Volcano plot of significantly down-regulated (blue) and up-regulated (red) genes in liver from mice as described in (A) ($|Log_2FC| > 1.5$, P value<0.01). (**D**) The nine-quadrant plot shows the correlation between differentially expressed proteins in the WAT and liver groups. (**E**) Heatmap analysis of differentially expressed genes in livers and WAT from vehicle- and HF-treated mice. (**F**) Reactome enrichment pathway analysis implicates GCN2/ATF4-associated cellular responses to stress pathway in HF-treated group. Significantly overrepresented pathways (FDR < 0.05) were grouped and depicted. The size of the circles corresponds to the number of genes in each module. (**G**) Levels of ATF4 protein in liver tissues of DIO mice injected with vehicle or HF (100 μg/kg), $n = 5$. (**H**) Serum GDF15 (vehicle group, $n = 7$; HF group, $n = 6$), FGF21 (vehicle group, $n = 7$; HF group, $n = 6$), leptin ($n = 7$), and adiponectin ($n = 7$) protein levels of DIO mice injected with HF (100 μg/kg) for 8 week. Data are means ± SEM. P values for the data of GDF15 and leptin were calculated by two-sided unpaired t tests. P values for the data of FGF21 and adiponectin were calculated by two-sided unpaired t tests with Welch's correction.

hepatocytes (*29*). Hence, we focused on the effects of HF on the GCN2/ATF4 signaling and the expression of GDF15 and FGF21 in the liver and hepatocytes. In DIO mice treated long-term with HF, there was an increase in ATF4 protein expression (Fig. 3G). Concurrently, circulating levels of GDF15 and FGF21 were elevated in both DIO mice and lean mice (Fig. 3H and fig.S5). In contrast, the differences in serum levels of other energy homeostasis-related hormones, including leptin and adiponectin were statistically insignificant (Fig. 3H). These studies demonstrate that HF treatment induces ISR in mouse liver and adipose tissues, leading to elevated levels of GDF15 and FGF21.

HF elevates GDF15 and FGF21 expression via ISR pathway

To determine whether HF can elevate GDF15 and FGF21 levels before weight loss effects occur, DIO mice were given short-term injections of HF (at intervals of 3, 6, and 12 hours). Our data demonstrate increased circulating levels of GDF15 and FGF21 post-acute HF treatment, with GDF15 levels peaking at 3 hours (Fig. 4, A and B). Moreover, we detected the expression of *Gdf15* and *Fgf21* genes in various tissues (including kidney, liver, ileum, iWAT, eWAT, iBAT, and skeletal muscle) of mice following a single intraperitoneal administration of vehicle or HF after 1 hour (Fig. 4C). The mRNA expression of *Gdf15* and *Fgf21* were similar between the two groups

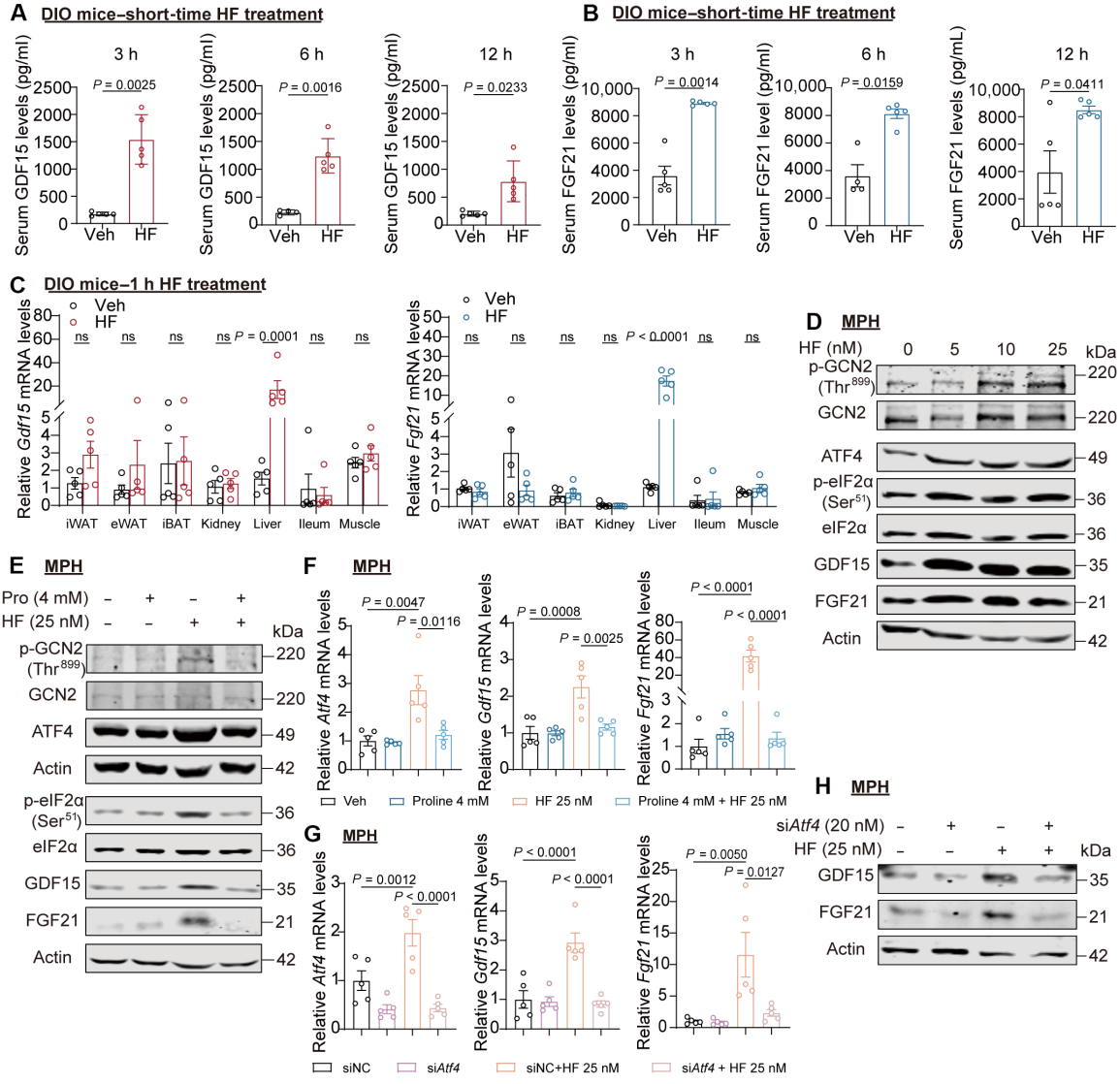

Fig. 4. HF elevates GDF15 and FGF21 expression via the ISR signaling pathway. (**A**) Serum GDF15 protein levels of DIO mice injected with HF (100 μg/kg) at indicated time [$n = 5$, except for the vehicle group at 6 hours ($n = 4$)]. (**B**) Serum FGF21 protein levels of DIO mice injected with HF (100 μg/kg) at indicated time [$n = 5$, except for the vehicle group at 6 hours ($n = 4$)]. (**C**) Levels of *Gdf15* and *Fgf21* mRNAs in indicated organs of DIO mice injected with vehicle or HF (100 μg/kg) at 1 hour ($n = 5$). (**D** and **E**) Protein levels (p-GCN2, GCN2, ATF4, p-eIF2α, eIF2α, GDF15, and FGF21) in mouse primary hepatocytes (MPH). (**F**) Levels of *Atf4*, *Gdf15*, and *Fgf21* mRNAs in MPH treated with HF (25 nM) in the presence or absence of proline (4 mM) for 24 hours ($n = 5$). (**G**) Levels of *Atf4*, *Gdf15*, and *Fgf21* mRNAs in control siRNA (si*NC*) or *Atf4* siRNA (si*Atf4*)–treated MPH exposed to HF (25 nM) ($n = 5$). (**H**) Protein levels (GDF15, and FGF21) in MPH. Data are presented as means ± SEM. Data in (A), 3 and 12 hours in (B) were calculated using two-sided unpaired *t* tests with Welch's correction. Data in 6 hours in (B) were analyzed by nonparametric tests. Bar graphs in (C) analyzed by two-way ANOVA followed by Bonferroni's multiple comparisons test. Data in (F) and (G) analyzed by two-way ANOVA followed by Tukey's multiple comparisons test.

in all organs except the liver where an up-regulation of *Gdf15* (fold change = 11) and *Fgf21* (fold change = 15.6) was observed in the HF group (Fig. 4C). In addition, in mouse primary hepatocytes (MPHs) and Huh-7 cells, HF induced the up-regulation of *ATF4*, *GDF15*, and *FGF21* gene expression and induced the phosphorylation of key ISR components, such as GCN2, eIF2α, as well as the increase of ATF4 (Fig. 4D and fig. S6, A and B). MAZ, as a negative compound, does not up-regulate the gene expression levels of *Atf4*, *Gdf15*, and *Fgf21* in MPHs (fig. S6C). The activation of ISR by HF is consistent with that reported in previous studies (*30*, *31*). However, the up-regulation of ATF4, GDF15, and FGF21 as well as GCN2 pathway was blocked by proline supplementation, indicating that amino acid responses play an essential role in HF–mediated pharmacological effects (Fig. 4, E and F, and fig. S6, D and E). In Huh-7 cells, inhibition of the ISR pathway reversed the gene up-regulation of *GDF15* and *FGF21* induced by HF (fig. S6F). Similarly, this effect was corroborated in vivo, where a single injection of ISRIB (an ISR inhibitor) (5 mg/kg), in combination with HF (100 μg/kg) treatment, reversed the up-regulation of *Gdf15* and *Fgf21* by HF in mice liver (fig. S6G). In the serum, ISRIB injection also reversed the HF-induced increase in GDF15 and FGF21 levels (fig. S6H). Further, *Atf4* depletion also rescues the up-regulation of *Gdf15* and *Fgf21* in mouse and human hepatocytes (Fig. 4, G and H, and fig. S6I). Thus, ISR is essential for the effects of HF on elevating GDF15 and FGF21.

GDF15 mediates the food intake suppression and weight-loss effect of HF

To test the involvement of GDF15 in mediating the effects of HF on weight loss, we used *Gdf15* knockout (KO) mice (Fig. 5A). Circulating levels of GDF15 in KO mice were undetectable, demonstrating complete KO of *Gdf15* (Fig. 5B). Ablation of *Gdf15* reversed the terminal weight-loss effect of HF by 27% and fat mass by 55% (Fig. 5, C and D). Furthermore, HF-induced reductions in iWAT mass in wild-type (WT) mice were reversed in *Gdf15* KO mice, consistent with the observed reduction in body weight (Fig. 5E). While HF treatment led to a decrease in plasma levels of TG and TC, these favorable effects were not observed in the absence of *Gdf15*, suggesting a pivotal role for *Gdf15* in mediating these impacts (Fig. 5F). In addition, the capacity of HF to reduce food intake was completely ablated in the absence of *Gdf15* (Fig. 5G). *Gdf15* KO did not alter the effects of HF on the up-regulation of UCP1 and energy expenditure (Fig. 5, H and I). In addition, while HF administration improved glucose tolerance and insulin sensitivity in WT mice, these metabolic benefits of HF were also evident in *Gdf15* KO mice, suggesting that *Gdf15* is not involved in mediating the effects of HF on glucose intolerance and insulin sensitivity (fig. S7, A and B). Collectively, these findings highlight the essential role of *Gdf15* in HF-mediated effects on obesity in mice while still indicating the existence of other mechanisms contributing to the metabolic benefits of HF.

FGF21 mediates the increased energy expenditure and weight-loss effect of HF

We conducted further investigations to ascertain whether hepatic FGF21 mediates the additional effects of HF on weight loss (Fig. 6A). We established hepatocyte-specific *Fgf21* KO mice (*Fgf21*$^{hep-/-}$ mice) through the crossbreeding of *Fgf21* $^{flox/flox}$ mice (WT mice) with Alb-cre mice, followed by administration of HF to both WT and *Fgf21*$^{hep-/-}$ mice. Circulating FGF21 levels were reduced to below 110 pg/ml (90% decrease) in hepatocyte-specific FGF21$^{hep-/-}$ mice, thereby confirming successful hepatocyte *Fgf21* deletion (Fig. 6B). Ablation of hepatic *Fgf21* reversed the terminal weight-loss effect of HF by 44% and that of fat mass by 53% (Fig. 6, C and D). Consistent with findings observed in *Gdf15* KO mice, HF administration reduced iWAT mass in WT mice; however, the effect of HF on iWAT loss was not observed in *Fgf21*$^{hep-/-}$ mice (Fig. 6E). Consistent with the reduction in body weight, HF treatment resulted in reduced plasma TG and TC levels. However, *Fgf21* hepatic deletion showed minimal impact on the lipid-lowering effect of HF (Fig. 6F). Notably, hepatic ablation of FGF21 did not reverse the ability of HF to reduce food intake (Fig. 6G) but inhibited the effects of HF on up-regulation of UCP1 and HF-elicited increase in energy expenditure (Fig. 6, H and I). HF-induced ameliorative effects on glucose intolerance and insulin resistance were mildly affected by hepatocyte-specific deletion of *Fgf21* (fig. S8, A and B). Collectively, these findings demonstrate the obligatory role of hepatocyte-derived *Fgf21* in the HF-mediated impact on weight loss.

The adverse reactions of HF

Because of reported side effects of HF and the limitations of rodents as a model for observing gastrointestinal (GI) adverse effects, we investigated the adverse effects of HF in beagles. Six beagles were administered a single oral dose of HF powder (0.56 mg/kg) in capsule form. Following the single dose, the dogs were continuously monitored for 24 hours, and the number of vomiting and diarrhea episodes was recorded for each dog. Both vomiting and diarrhea occurred within 8 hours post-administration. The incidence of vomiting was observed in 33% of the dogs, while diarrhea was observed in 100% of the dogs (fig. S9). These results suggest that HF induces GI adverse reactions in beagles, with diarrhea being the most prevalent side effect.

DISCUSSION

In the present study, we identified HF, a derivative of the antimalarial quinazolinone natural product alkaloid, febrifugine, as an inducer of ISR-dependent elevation of endogenous GDF15 and FGF21, which regulate food intake and energy expenditure and hence lowers body weight. These pharmacological, metabolic, and mechanistic data support the potential of HF for treating obesity and its comorbidities. The AAS response, triggered by endogenous amino acid depletion, activates metabolic regulation mechanisms that remain understudied. In this regard, inhibition of EPRS by HF leads to the accumulation of uncharged tRNAs, initiating autophosphorylation of the amino acid sensor GCN2, resulting in the phosphorylation of eIF2α and increased expression of ATF4. The involvement of the GCN2 pathway in various metabolic processes has already been documented (*32*, *33*). GCN2 plays a complex and context-dependent role in regulating metabolic processes, with distinct effects depending on the nutritional state of the organism. Under conditions of nutrient sufficiency, particularly when amino acids are abundant, the absence of GCN2 has been shown to confer widespread metabolic benefits (*34*–*36*). In contrast, under conditions of amino acid deprivation or pharmacological inhibition, GCN2 activation is crucial for maintaining physiological balance. These molecular events induce a wide array of adaptive responses aimed at conserving energy, protecting cells from oxidative stress, and promoting survival during periods of nutrient scarcity. In such stress situations, GCN2 activation helps to reprogram gene expression to favor catabolic processes, preparing the organism to better cope with nutrient deficit (*37*, *38*).

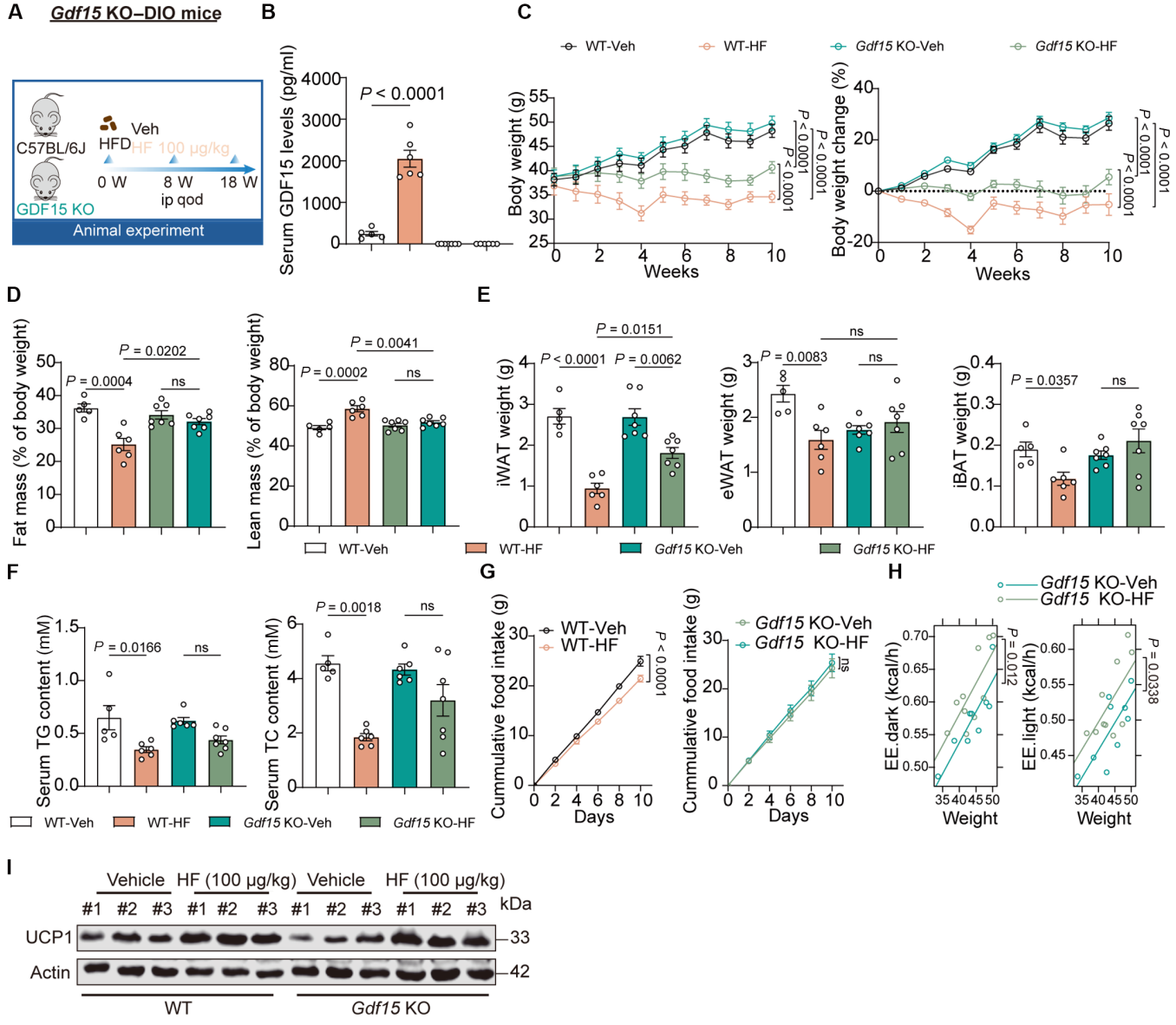

Fig. 5. GDF15 mediates weight-loss effect of HF by inhibiting food intake. (**A** to **F**) Eight-week-old male WT and *Gdf15* KO mice were fed with HFD for 8 weeks. WT and *Gdf15* KO mice were then randomly assigned to vehicle or HF (100 μg/kg) group and injected every 2 days for 8 weeks. (B) Serum GDF15 levels. (C) Body weight and % body weight change (WT-Veh, $n = 5$; WT-HF, $n = 6$; *Gdf15* KO-Veh, $n = 7$; *Gdf15* KO-HF, $n = 7$). (D) Fat mass and lean mass (% body weight). (E) Weights of adipose tissues. (F) Serum TC and TG levels (WT-Veh, $n = 5$; WT-HF, $n = 6$; *Gdf15* KO-Veh, $n = 6$; *Gdf15* KO-HF, $n = 7$). (**G**) Cumulative food intake of single cage WT or *Gdf15* KO mice treated with vehicle or HF (100 μg/kg) ($n = 4$). (**H**) EE in *Gdf15* KO mice treated with vehicle or HF (100 μg/kg) (vehicle group, $n = 9$; HF group, $n = 10$). (**I**) UCP1 protein abundance in iBAT of HF (100 μg/kg)–treated WT and *Gdf15* KO mice ($n = 3$). Data are presented as means ± SEM. Data in (B) to (F) were determined through two-way ANOVA followed by Bonferroni's multiple comparisons test. Data in (G) were determined through two-way ANOVA. Data in (H) were determined through ANCOVA using body mass as a covariate.

This dual role underscores the importance of GCN2 in maintaining metabolic homeostasis and highlights its potential as a therapeutic target for metabolic diseases associated with nutrient imbalance, such as obesity, diabetes, and liver disorders.

Obesity and related metabolic abnormalities are commonly attributed to energy imbalance due to excess food (calorie) intake and/or insufficient physical activity (*1*, *2*). The therapeutic potential of GDF15 and FGF21 in obesity and metabolic liver diseases has been explored in preclinical studies and clinical trials (*39*–*42*). For example, a long-acting GDF15 analog showed promising results in obese Cynomolgus monkeys, leading to 16 ± 5% weight loss (*43*). More recently, artesunate has been reported to treat obesity in mice and nonhuman primates through GDF15/GFRAL signaling axis (*44*). Notably, GDF15 analogs have induced significant weight loss in rodents and monkeys; however, these effects have not yet been successfully translated to human weight loss outcomes (*45*, *46*). The development of GDF15 as a therapeutic agent is thus still in its infancy. Beyond GDF15, FGF21 analogs have also shown beneficial

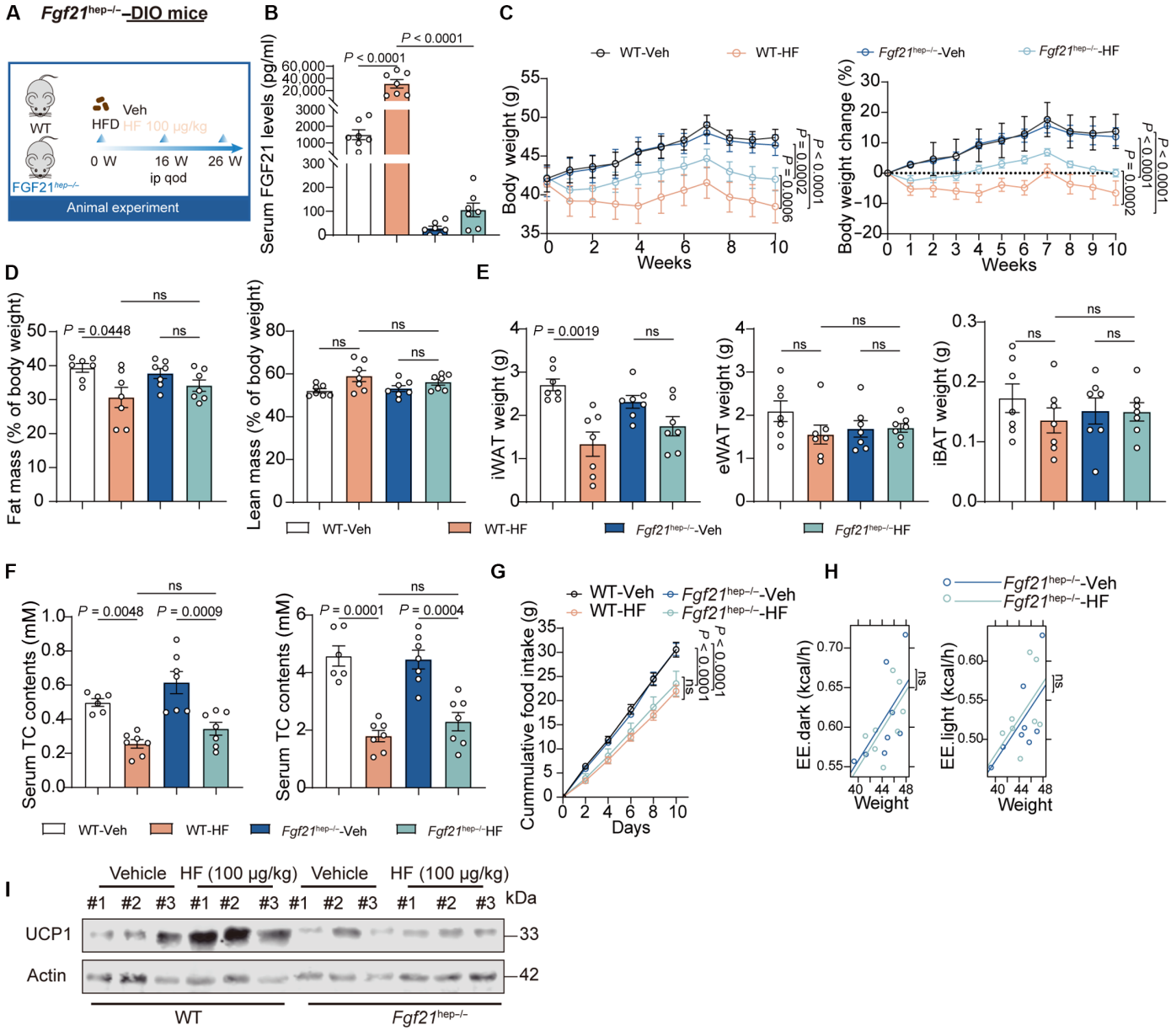

Fig. 6. FGF21 mediates weight-loss effect of HF by increasing energy expenditure. (**A** to **F**) Eight-week-old male *Fgf21*$^{flox/flox}$ mice (WT) and *Fgf21*$^{hep-/-}$ mice were fed with HFD for 16 weeks and then randomly divided into vehicle or HF (100 μg/kg) group and injected every 2 days for 10 weeks. (B) Serum FGF21 levels ($n = 7$). (C) Body weight and % body weight change ($n = 7$). (D) Fat mass and lean mass (% body weight) ($n = 7$). (E) Weights of adipose tissues ($n = 7$). (F) Serum TC and TG levels (Veh, $n = 6$; other group, $n = 7$). (**G**) Cumulative food intake of single cage WT or *Fgf21*$^{hep-/-}$ mice treated with vehicle or HF (100 μg/kg) ($n = 4$). (**H**) EE in *Fgf21*$^{hep-/-}$ mice treated with vehicle or HF (100 μg/kg) (vehicle group, $n = 8$; HF group, $n = 8$). (**I**) UCP1 protein abundance in BAT of HF (100 μg/kg)–treated WT and *Fgf21*$^{hep-/-}$ mice ($n = 3$). Data are presented as mean ± SEM. Data in (B) to (G) were determined through two-way ANOVA by Bonferroni's multiple comparisons test. Data in (H) were determined through ANCOVA using body mass as a covariate.

effects on lipid metabolism and liver function, rendering them as promising candidates for treating metabolic disorders, including metabolic liver diseases. The phase 2 clinical trial results for pegozafermin, an FGF21 analog, indicated that, after 24 weeks, the highest-dose group demonstrates a one-stage or better improvement in liver fibrosis (*47*). In this study, we observed that HF rapidly increased serum levels of GDF15 and FGF21, mediated by the canonical ATF4-dependent ISR pathway. In vitro, the supplementation of proline in hepatocytes negated HF-induced increase in GDF15 and FGF21. In vivo data obtained with MAZ1310 treatment of obese mice provided additional support for the involvement of EPRS inhibition in HF-induced weight loss effects.

Previous work have shown that GDF15 reduces appetite, enhances energy expenditure in muscle, and thereby reduces body weight (*28*, *48*, *49*), while FGF21 administration enhances energy expenditure, boosting insulin sensitivity and resulting in weight loss, partially independent of effects on food intake (*50*, *51*). However, clinical trials using protein-based therapies face challenges in

improving metabolic disorders due to protein stability, administration methods, and patient adherence to treatment regimens. As a potential therapeutic agent, GDF15 encounters obstacles in terms of druggability. For example, GDF15 has a very short half-life, approximately 3 hours in both mice and Cynomolgus monkeys (*52*). Moreover, GDF15 exhibits a strong propensity to aggregate, leading to low stability and expression titers. In contrast, HF has advantage and effectively acts as a pharmaco-mimetic of AAR by stimulating endogenous secretion of GDF15 and FGF21 and maintaining elevated circulating levels of both metabolic hormones for extended periods. This could be a useful approach for the therapy of obesity-associated metabolic disorders based on the simultaneous action of these two proteins stimulated by a single drug, which is expected to circumvent the shortcomings of protein analogs of GDF15 and FGF21. In addition to HF, other intervention strategies, such as iD1 (*26*) (a pharmacological inhibitor of CNOT6L deadenylase), and dietary intervention (ketogenic diet) (*53*), have been reported to activate GDF15 and FGF21, leading to weight loss and amelioration of metabolic disorders. These findings are in harmony with ours. Specifically, ID1 enhances the levels of GDF15 and FGF21 through inhibiting the action of CNOT6L (*26*), while the ketogenic diet primarily exerts its beneficial effects via hepatic PPARγ (*53*). This convergence of different mechanisms underscores the pivotal roles of GDF15 and FGF21 in maintaining energy homeostasis and metabolic health. Despite targeting different pathways, these interventions achieve similar outcomes, highlighting the versatility and importance of GDF15 and FGF21 in addressing metabolic diseases.

Our results reveal a different regulatory mechanism of HF in lean versus obese mice. In lean mice, HF treatment up-regulated GDF15 and FGF21, key metabolic regulators known to influence appetite control, resulting in suppressed food intake. However, HF did not enhance energy expenditure in lean mice, suggesting a more limited metabolic effect under lean conditions. On the other hand, in obese mice, HF not only up-regulated GDF15 and FGF21 to suppress appetite but also significantly increased energy expenditure. This dual action in obese mice may reflect a greater metabolic flexibility or responsiveness to HF in states of energy surplus, potentially involving pathways related to thermogenesis and/or increased activity of brown adipose tissue.

HF shows potential for translation into an anti-obesity treatment based on its versatile pharmacological actions and acceptable safety when used at low-dose. Previous studies have reported HF's antimalarial, anti-inflammatory, anti-fibrotic, anticancer, and antiviral effects, supporting its clinical translational value due to its polypharmacological actions (*14*, *16*–*18*). Further, clinical trials of HF have centered on evaluating its efficacy for HIV-related Kaposi's sarcoma and advanced solid tumors (www.clinicaltrials.gov). In phase 1 and II clinical trials, the recommended oral dose of HF for long-term administration is 0.5 mg/day (*19*, *20*). In our experiments, the dose of HF recommended for anti-obesity purposes (100 μg/kg) is approximately half of the lowest dose tested in phase 2 clinical trials and even lower doses of HF (25 μg/kg or 50 μg/kg) have been effective in controlling body weight in mice. Also, in nonobese animals fed a standard chow diet, HF administration had no notable adverse effects in major tissues, another assurance of its safety.

Intriguingly, one earlier and independent study by Rai *et al.* (*30*) has reported similar phenotype of HF-treated obese mice. We demonstrate HF's potential as a therapeutic agent for obesity and metabolic syndrome, including weight reduction, improved insulin resistance, and decreased serum insulin levels. While different from our study, no statistically significant difference in food consumption was observed in the study by Rai *et al.* (*30*). One plausible explanation may be the different drug dosages, routes of administration, drug intervention frequency, and methods used to calculate food consumption between this study and ours. The fact that inhibition of the PERK branch of ISR by GSK2656157 did not fully recapitulate the opposite phenotype of HF suggests that GCN2- and PERK-dependent ISR have some overlapping but not identical roles in regulating insulin resistance and obesity. Notably, while the previous study used a PERK inhibitor to target upstream ISR signaling, our study used a direct ISR inhibitor (ISRIB), which effectively reversed the HF-induced increase in GDF15 and FGF21 levels in an acute mouse experiment. This finding highlights the crucial role of ISR in mediating the metabolic effects of HF. Together, both studies consolidate the reproducible phenotype of HF in preventing obesity. A recent study examined (*54*) the effects of direct ISR activation using small molecule activators and found that activating the ISR pathway led to a reduction in obesity and improved metabolic outcomes in mice. This aligns with our findings, where HF, through its effect on the ISR pathway, influenced body weight and food intake in a similar manner. In addition, another study (*55*) investigated the effects of a low-protein diet (LPD) on ISR induction and its role in obesity and demonstrated that LPD-induced ISR activation promoted adaptive responses to nutrient scarcity and was associated with improved weight control and insulin sensitivity. This contrasts with the typical obesogenic effects of high-protein or HFDs. While our study does not specifically involve an LPD, the underlying mechanisms of ISR induction in response to dietary changes could be relevant to understanding how HF influences obesity-related pathways.

We observed that the beneficial effects of HF treatment on glucose metabolism persist in both *Gdf15* KO and *Fgf21*$^{hep-/-}$ mice. We speculate that these effects are due to the independent actions of GDF15 (*56*) and FGF21 (*29*) in improving glucose metabolism. In the case of single-gene KO, we might not observe a complete reversal of glucose tolerance improvement, as the effects of GDF15 and FGF21 could be complementary but not fully compensate the absence of one factor. Another study has also discussed the reciprocal influence between GDF15 and FGF21 (*57*). In addition, we considered the possibility that other factors, beyond GDF15 and FGF21, might also contribute to the observed metabolic improvements by HF. The activation of the ISR pathway may have other effects, either directly or indirectly, that contribute to the improvement of insulin resistance by HF (*30*, *54*, *55*). This potential involvement of additional mechanisms warrants further investigation.

Noteworthy, we observed that HF administration induced GI adverse effects, including nausea and vomiting, in canine models. This finding aligns with previous studies (*19*, *21*) reporting GI intolerance as a common side effect of HF and its analogs, which could limit their clinical application. We propose potential strategies to mitigate the adverse effects of HF either by chemical modification of HF to improve its tolerability while preserving its therapeutic efficacy or by combined use with antiemetics in future clinical trials.

Although HF improved the metabolic traits of obese mice, caution must be exercised as pharmacologically modulating AAS pathways may have broad impacts on cellular functions beyond metabolism. In addition, given the broad-spectrum effects of HF as well as the fact that GDF15 release in circulation is drug, tissue, and disease stage specific, the major contributor to the increase in circulating GDF15 in

response to HF treatment warrants further verification in liver-, gut-, adipose tissue–, or kidney-specific *Gdf15*–deficient mice. Also, to claim that HF curbs obesity in DIO mice in a GDF15/GFRAL signaling–dependent manner, genetic ablation or neutralization of GFRAL is necessary. Last but not least, in mice deficient of both hepatic *Gdf15* and *Fgf21*, it is needed to clarify whether the anti-obese effects of HF depend on dual contribution of *Gdf15* and *Fgf21*.

In summary, we report HF as a potential therapeutic drug to curb diet-induced obesity and metabolic disorders through suppressing food intake and increasing energy expenditure. The actions of HF are dependent on pharmacological increase of endogenous metabokines GDF15 and FGF21. Future clinical studies are warranted to determine the therapeutic actions of HF in patients with obesity and metabolic diseases, as well as define the long-term safety profile of activating AAS response pharmacologically.

MATERIALS AND METHODS

Animal studies

All experimental procedures were conducted in accordance with the National Institutes of Health "Guide for the Care and Use of Laboratory Animals." Approval for the animal experiments was granted by the Institutional Animal Care and Use Committee [approval number for mouse experiments: USTCACUC27120124062, approval number for pig and dog experiments: 2023-N(A)-0172]. Eight-week-old C57BL/6J mice (strain no. N000013) and *ob/ob* mice (strain no. T001461) were obtained from GemPharmatech (Nanjing, China). Male C57BL/6J mice with 7- to 15-week HFD-induced obesity (strain no. T002040) were purchased from GemPharmatech. During the induction period, the mice were housed in a specific pathogen–free (SPF) facility under controlled conditions (temperature: 20° to 26°C, relative humidity: 40 to 70%). Mice meeting the experimental criteria (defined as those with a body weight 20 to 25% greater than that of the control group) were placed in transport cages containing bedding, agar, and food and were transported to the animal facility at the University of Science and Technology of China via an animal transport vehicle. After 1 week of acclimation, experiments were conducted (mouse experiments 1, 2, 3, 6, 8, and 9). *Gdf15*$^{-/-}$ (strain no. T011862) (*58*, *59*) and *Alb-cre* (strain no. T003814) mice were purchased from GemPharmatech (Nanjing, China). *Fgf21*$^{flox/flox}$ (NM-CKO-00136) mice were purchased from Shanghai Model Organisms Center (Shanghai, China). The mice were housed in an SPF environment with 12 hours of light and 12 hours of dark cycle and were maintained at 23° ± 2°C with free access to food (maintenance diet for mice and rats, Wonder-journey Co., Wuhan, China; 4% fat, 20% protein) and water. The animals were randomly assigned into different groups before being subjected to HFD (D12492, Research Diets, NJ, USA). Bama miniature pigs and beagle were purchased from Zhenjiang Wanwei Co. (Zhenjiang, China). Six-month-old pigs (healthy and passed the local quarantine inspection) and 12-month-old dogs were housed in large animal facility with free access to water.

Drug treatment

For HF treatment, the mice received different doses of HF (T3524, Targetmol, MA, USA) or vehicle [0.1% dimethyl sulfoxide (DMSO) mixed with physiological saline] intraperitoneally according to the different experimental requirements until the end of the experiment. For liraglutide treatment, liraglutide (6 mg/ml, Novo nordisk, Victoza, Liraglutide Injection, Bagsværd, Denmark) was diluted with physiological saline containing 0.1% DMSO to a final concentration of 0.06 mg/ml, ensuring consistent injection volumes with the HF and vehicle groups. In the oral administration experiment, the vehicle consisted of 50% polyethylene glycol, molecular weight 400 (PEG-400), 0.2% DMSO, and physiological saline. Orlistat (T0686, Targetmol, MA, USA) was dissolved in PEG-400, followed by the addition of 0.2% DMSO and physiological saline. The mixture was thoroughly ultrasonicated to form a homogenous suspension before being administered via oral gavage. For ISRIB treatment, ISRIB (HY-12495A, MedChemExpress, NJ, USA) was dissolved in 10% DMSO, 50% PEG-400, and 40% physiological saline. The solvents in the HF group and the vehicle group were the same. Drugs of stock solution were aliquoted and stored at −80°C. Fresh working solution was made before used.

Animal experiments

Pig experiment: Study of HF in pigs

To expedite the development of obesity in pigs, HFD (containing 10% lard, 14% margarine, 10% sucrose, 1.5% cholesterol, and 0.5% sodium cholate) (*60*) was provided (XT19031, Jiangsu Xietong Co., Nanjing, China). Bama miniature pigs were randomly assigned to three groups: One group received a chow diet (XTC06WC, Jiangsu Xietong Co., Nanjing, China), one group received an HFD, and another group was given an HFD supplemented with HF (1.85 mg/kg, w/w). This dose was calculated on the basis of the conversion between mice and pigs as well as the daily food consumption rate of pigs. The body weights of the pigs were recorded at the beginning and 16 weeks after HFD feeding.

Dog experiment: Study of HF in dogs

Six beagle dogs, each weighing approximately 12 kg, were administered a single oral dose of HF powder encapsulated in capsules (0.56 mg/kg). They were monitored continuously for 24 hours, and the number of vomiting and diarrhea episodes in each dog was recorded. The incidence of vomiting/diarrhea was calculated.

Mouse experiment 1: Effect of HF on DIO mice

Mice (8-week-old male C57BL/6J) were fed an HFD for 16 weeks and then randomly assigned to five experimental groups: (i) vehicle group, (ii) HF (25 μg/kg) treatment group, (iii) HF (50 μg/kg) treatment group or (iv) HF (100 μg/kg) treatment group, with five mice per group, and (v) liraglutide (200 μg/kg) (a GLP1R agonist, reference drug) treatment group with four mice per group. The mice were fed an HFD for 8 weeks and treated with intraperitoneal injections of vehicle, HF, or liraglutide every 2 days. The body weights were monitored weekly. After receiving treatment for 8 weeks, the mice were euthanized after starvation overnight.

Mouse experiment 2: HF withdrawal experiment

Mice (8-week-old male C57BL/6J) on an HFD for 12 weeks were randomly assigned into two groups: (i) vehicle group ($n = 10$) or (ii) HF (100 μg/kg) treatment group ($n = 20$). The mice were injected with vehicle and HF every 2 days for 6 weeks, and then the HF group was randomly divided into two groups: (i) continuous administration group ($n = 10$) and (ii) withdrawal group ($n = 10$). The body weights were monitored weekly.

Mouse experiment 3: Effect of HF on DIO mice under TN conditions

Mice (8-week-old male C57BL/6J) on an HFD for 12 weeks were randomly assigned into two groups: (i) vehicle group ($n = 8$) or (ii) HF (100 μg/kg) treatment group ($n = 8$). During the 2 weeks

preceding the experiment, mice subjected to high-fat feeding for 10 weeks were transferred from a 23°C environment to a temperature-controlled incubator maintained at 30°C. Following a 2-week acclimatization period, drug administration was initiated. The mice were treated with intraperitoneal injections of vehicle and HF every 2 days for 20 days.

Mouse experiment 4: Effect of HF on ob/ob mice

Male *ob/ob* mice (8-week-old) were raised under a standard chow diet and randomly assigned into two groups: (i) vehicle ($n = 7$) or (ii) HF (100 μg/kg) treatment group ($n = 8$). The mice were treated with intraperitoneal injections of vehicle and HF every 2 days. The animals were weighed weekly. At the end of 8-week testing, the mice were euthanized after starvation overnight.

Mouse experiment 5: Effect of HF on lean mice

To monitor the chronic safety of long-term treatment with HF, male 8-week-old C57BL/6J mice were injected intraperitoneally with vehicle or HF (100 μg/kg) every 2 days for 28 weeks. Body weights were monitored every week. At the end of experiment, the mice were euthanized by anesthesia after starvation overnight.

Mouse experiment 6: Effect of oral HF treatment on DIO mice

Mice (8-week-old male C57BL/6J) were randomly assigned into five experimental groups: (i) normal diet control, (ii) HFD vehicle control, (iii) HFD + HF (100 μg/kg), (iv) HFD + HF (200 μg/kg), and (v) HFD + orlistat (20 mg/kg) (an orally bioavailable anti-obesity reference drug). After 12 weeks of normal diet or HFD feeding, the mice were treated with vehicle or HF every 2 days by oral gavage.

Mouse experiment 7: Effect of HF on female mice

Mice (8-week-old female C57BL/6J) were fed HFD for 20 weeks and then randomly assigned to two groups: (i) vehicle group ($n = 5$) and (ii) HF (100 μg/kg) treatment group ($n = 5$). The body weights were monitored weekly.

Mouse experiment 8: Pair feeding

Mice (8-week-old male C57BL/6J) with HFD for 12 weeks were randomly divided into three groups: (i) vehicle group ($n = 8$), (ii) HF (100 μg/kg) treatment group ($n = 8$), and (iii) pair-fed vehicle group ($n = 8$). Pair-fed vehicle-treated mice received the same amount of food as ingested by the corresponding HF-treated groups the day before. Body weight and food intake were recorded daily.

Mouse experiment 9: Short-term HF treatment

Mice (8-week-old male C57BL/6J), fed HFD for 12 weeks, were euthanized at 1, 3, 6, and 12 hours post a single treatment with vehicle or HF.

Mouse experiment 10: ISR inhibition experiment

Eight-week-old male C57BL/6J mice were randomly divided into three groups: (i) vehicle group ($n = 4$), (ii) HF (100 μg/kg) treatment group ($n = 4$), and (iii) HF (100 μg/kg) treatment group + ISRIB (5 mg/kg) treatment group ($n = 4$). Dosage of ISRB was selected on the basis of published literature. At the beginning of the experiment, a single acute intraperitoneal injection of ISRIB at 5 mg/kg and vehicle was administered. After 20 min, on the basis of the grouping, the mice were injected with HF (100 μg/kg) or solvent. After 3 hours, the mice were euthanized, and the liver and serum were collected.

Mouse experiment 11: Effect of HF in Gdf15$^{-/-}$ mice

Eight-week-old male C57BL/6J mice (WT) and *Gdf15*$^{-/-}$ mice were fed with HFD for 8 weeks. Deletion of *Gdf15* was confirmed by genotyping and enzyme-linked immunosorbent assay (ELISA) of circulating GDF15 levels. WT and *Gdf15*$^{-/-}$ mice were then randomly assigned to vehicle or HF (100 μg/kg) group and injected every 2 days for 10 weeks. The mice were monitored weekly for body weight and food intake and then were euthanized by anesthesia after starvation overnight after 10 weeks of HF treatment.

Mouse experiment 12: Effect of HF in Fgf21$^{hep-/-}$ mice

Fgf21$^{hep-/-}$ mice were obtained by were crossing *Fgf21*$^{flox/flox}$ mice with *Alb-cre* mice. Deletion of hepatic *Fgf21* was confirmed by genotyping and ELISA of circulating FGF21 levels. Eight-week-old male *Fgf21*$^{flox/flox}$ mice (WT) and *Fgf21*$^{hep-/-}$ mice were fed with HFD for 16 weeks and then randomly divided into vehicle or HF (100 μg/kg) group. The mice were injected intraperitoneally every 2 days for 10 weeks and were euthanized at the end of experiment.

Fasting-refeeding protocol

The fasting-refeeding studies were performed in 12-week HFD mice. The experimental methodology was adapted from previously published literature (*25*). To minimize stress and ensure accurate measurements, the mice were acclimated to individual housing in single cages for 48 hours before the start of the experiment. Following the acclimation period, the mice underwent a fasting period of 16 hours, during which all food was removed to standardize baseline metabolic conditions. One hour after receiving the HF treatment, food was reintroduced to the cages, and the mice were allowed to feed freely. Food intake was carefully monitored and recorded at 1, 2, 3, and 4 hours post-refeeding.

Pharmacokinetics and tissue distribution of HF

For pharmacokinetic studies, after a single intravenous (168 μg/kg) or oral administration (840 μg/kg) of HF in male ICR mice ($n = 3$ per group), plasma samples were collected at indicated time points (0.25, 0.5, 1, 2, 4, 8, and 24 hours) to measure HF concentrations by high-performance liquid chromatography. For tissue distribution studies, after a single intravenous (168 μg/kg) or oral administration (840 μg/kg) of HF in ICR mice, the mice were euthanized and their plasma and tissues were collected at indicated time points (0.25, 2, 4, and 8 hours) to measure HF concentrations.

Cold exposure test

For cold exposure experiments (*61*), mice were exposed to 6°C to test their cold tolerance. The core body temperatures were recorded by a rectal thermometer (Physitemp, Clifton, NJ) at 0, 1, 2, 4, and 6 hours. The mice had free access to water but not to food. The aforementioned experiments were performed on mice (8-week-old male C57BL/6J) fed an HFD for 12 weeks.

Glucose tolerance test and insulin tolerance test

For glucose tolerance test, mice were fasted overnight for 16 hours (17:00 p.m. to 9:00 a.m.) and received intraperitoneal injection of D (+)-glucose (Diamond, A100188, Shanghai, China) solution in saline (2 g/kg body weight). Blood glucose levels were measured from the tail vein by glucometer (Vivachek, VGM83, Hangzhou, China) at 0, 15, 30, 60, 90, and 120 min after injection. For insulin tolerance test, the mice were intraperitoneally injected with insulin (0.75 U/kg; Novorapid, Insulin Aspart Injection, Bagsværd, Denmark) after 4 hours of fast (9:00 a.m. to 13:00 p.m.). Blood glucose levels were measured at 0, 15, 45, 30, 60, 90, and 120 min. The experiments described above were conducted in mouse experiment 1, 7, 10, and 11.

Blood tests

Blood was collected and placed in anticoagulant tubes (50 μl) and microcentrifuges tubes (about 600 μl), respectively. Fresh blood in

the anticoagulant tubes was immediately analyzed for blood cell content using an automated blood analyzer (Mindray, BC-30 Vet, Shenzhen, China). The blood in the microcentrifuge tubes were left at room temperature for 2 hours, centrifuged at 2000*g* for 15 min, and the serum was collected and stored in the refrigerator at −80°C. The serum parameters include ALT, AST, TG, TC, high-density lipoprotein, low-density lipoprotein, urea, and CREA were measured by using assay kits (Rayto, Shenzhen, China). Levels of mouse serum GDF15 were measured by the Mouse/Rat GDF-15 Quantikine ELISA Kit (R&D Systems, MGD150, MN, USA). Levels of mouse serum FGF21 were assessed by the Mouse/Rat FGF21 Quantikine ELISA Kit (R&D Systems, MF2100, Minnesota, USA). Levels of insulin were detected by the Mouse Insulin ELISA Kit (Mercodia, 10-1247-01, Uppsala, Sweden).

Body composition measurements

Total lean mass and fat mass of mice after treatment of either vehicle or HF were assessed using Minispec (Bruker, Massachusetts, USA).

In vitro translation experiment with rabbit reticulocytes

The Flexi Rabbit Reticulocyte Lysate System kit from Promega (L4540, WI, USA) was used for the experiments per the user guide. In summary, all required components for in vitro translation were prepared in a microcentrifuge tubes, with a final concentration of 200 nM HF, 200 nM MAZ1310, or 8 mM proline. The reaction mixture was incubated at 30°C for 90 min, followed by the measurement of luciferase activity.

Liver TG and TC analysis

To quantify the levels of hepatic lipids, liver tissue samples were first weighed and then homogenized in 1 ml of lysis solution (chloroform:methanol = 2:1). Steel beads were added, and the samples were ground using a tissue homogenizer (Shanghai Jingxin, JXFSTPRP-24 L, Shanghai, China) at 60 Hz for 120 s. After grinding, the samples were left at room temperature for 10 min and vortexed every 5 min to ensure proper mixing. Following this, 200 μl of phosphate-buffered saline was added to the extract, and the mixture was vortexed vigorously before being incubated at room temperature for another 10 min. The samples were then centrifuged at 1500*g* for 20 min. The lower phase (approximately 200 μl) was carefully transferred into a new 1.5-ml microcentrifuge tube. The solvent was evaporated under open conditions at 50°C for approximately 1 hour. Last, 200 μl of isopropanol was added, and the sample was dissolved at room temperature for at least 1 hour or overnight at 4°C on a shaking platform. The TG and TC levels were then quantified using commercial assay kits (Wako, 632-50991 and 635-50981, Osaka, Japan) according to the manufacturer's instructions.

Metabolic chamber

Food intake, oxygen consumption, and energy expenditure were determined with CLAMS (Columbus, Ohio, USA). Mice were individually housed and acclimated to the metabolic chambers for 3 days. Before formal testing, the mice were injected intraperitoneally with saline every day for 3 days. Then, vehicle or HF (100 μg/kg) were administered to mice every 2 days before dark cycle. Oxygen consumption and the RER were measured following the protocol provided by the manufacturer (Columbus Instruments). Oxygen consumption was expressed as the rate of O_2 consumed per kilogram of body weight per hour. The RER was calculated using the following equation: RER = VCO_2/VO_2, where VCO_2 is the rate of carbon dioxide production and VO_2 is the rate of oxygen consumption. Heat production was also calculated on the basis of these parameters. Hourly data were statistically analyzed using CalR (https://CalRapp.org/) (*62*), and analysis of covariance (ANCOVA) was performed with R Studio.

Cell culture

Huh-7 cells (Cellbank, SCSP-526, Shanghai, China) were seeded at a density of 1×10^5 cells per well in 12-well plates and cultured in Dulbecco's minimum essential medium (DMEM, KeyGEN biotech, KGL1206-500, Nanjing, China) supplemented with 10% fetal bovine serum (FBS, Sigma-Aldrich, F7524, Missouri, USA). Cells in 12-well plates were used for drug treatment and small interfering RNA (siRNA) knockdown with treatment duration of 24 hours. Transfection was performed when the cells reached approximately 70% confluence, and siRNA was transfected at a concentration of 20 nM using Lipofectamine 2000 (Thermo Fisher Scientific, 11668019, MA, USA). Transfection was performed according to the manufacturer's instructions. Briefly, before transfection, the culture medium was replaced with 700 μl of Opti-MEM (Thermo Fisher Scientific, 31985070, Massachusetts, USA). Then, siRNA and Lipofectamine 2000 were each added to 150 μl of Opti-MEM, incubated for 5 min, mixed together, and left to sit for 20 min before adding to the cells (final volume of 1 ml). In transfection experiments, the cells were treated with drugs for an additional 24 hours following 24 hours of siRNA transfection. At the end of the experiment, cellular RNA and proteins were extracted. RNA extraction was performed according to the manufacturer's instructions (ESScience, RN001, Shanghai, China). For protein extraction, 150 μl of 1 × SDS–polyacrylamide gel electrophoresis (SDS-PAGE) protein loading buffer (Beyotime, P0015L, Shanghai, China) was added to each well. After complete cell lysis, the samples were collected into microcentrifuge tubes, denatured at 95°C for 10 min, and stored at −80°C for subsequent experiments. The experiments in Huh-7 cells were performed with three to five biological replicates. siRNA sequences are available in table S1.

Isolation and culture of primary mouse hepatocytes

MPHs were isolated from 8-week-old male C57BL/6J mice following established protocols, as detailed in our previous methodology (*63*). In brief, the mice were anesthetized and the liver was perfused with a buffer containing 137 mM NaCl, 5.4 mM KCl, 0.5 mM NaH_2PO_4, 0.4 mM Na_2HPO_4, 4.2 mM $NaHCO_3$, 0.5 mM EGTA, and 5 mM glucose (pH 7.4) at 5 ml/min via the inferior vena cava. After the initial perfusion, a digestion solution with 0.04% collagenase IV (Diamond, A004186, Shanghai, China) was injected into the liver. After 20 min of perfusion, the liver tissue was enzymatically digested, and the released hepatocytes were separated using a 70-μm cell strainer to remove any undigested debris. The hepatocytes were plated onto collagen-coated dishes and cultured in DMEM with 10% FBS and 1% penicillin-streptomycin at 37°C in a humidified incubator with 5% CO_2. Adherent primary hepatocytes exhibit the typical binucleated feature of mammalian hepatocytes and display a distinct hexagonal "chicken wire" shape after 12 hours of adhesion. In addition, we confirmed the identity of the isolated cells as hepatocytes through quantitative PCR (qPCR) analysis of hepatocyte-specific gene expression, such as *Alb* and *Tbg*. For drug treatment and siRNA-mediated gene knockdown experiments, the cells were seeded in 12-well plates at a density of 1×10^5 cells per well and incubated for 4 hours before treatment. The experimental methods for

drug treatment and siRNA transfection were consistent with those used for Huh-7 cells. RNA and proteins were collected and stored at −80°C for subsequent experiments. The experiments in MPH were performed with three to five biological replicates. siRNA sequences are available in table S1.

Histological analysis

Freshly harvested tissues were promptly fixed in 4% paraformaldehyde overnight to preserve cellular architecture and protein integrity. Following fixation, the tissues were embedded in paraffin wax. The paraffin-embedded samples were then sectioned at a thickness of 5 to 10 μm using a microtome. For histological examination, the tissue sections underwent hematoxylin and eosin staining.

Adipocyte area analysis

Randomly selected optical fields from histological images of different mice were used for quantification of adipocyte area. Adipocytes were counted, and their average area was calculated using ImageJ software by dividing the total area of the region by the number of cells. The average adipocyte area for each mouse was then used for graphical representation.

Western blotting

Approximately 20 mg of tissue was weighed, and radioimmunoprecipitation assay buffer (Sangon, C500005-0100, Shanghai, China) supplemented with 1× protease inhibitor (Yeasen, 20124ES03, Shanghai, China) and phosphatase inhibitor (Yeasen, 20109ES05, Shanghai, China) was added. The tissue was then homogenized using a homogenizer (Shanghai Jingxin, JXFSTPRP-24L, Shanghai, China) at 60 Hz for 180 s, thoroughly disrupted, and incubated on ice for 30 min followed by centrifugation at 12,000*g* for 10 min. The resulting supernatants were harvested, and the total protein content was determined using a BCA Protein Assay Kit (Thermo Fisher Scientific, 23235, MA, USA). Subsequently, protein extract (2 mg/ml) was mixed with loading buffer and subjected to denaturation through boiling at 95°C for 10 min. Equal quantities of protein were separated via electrophoresis on either 10 or 12% SDS-PAGE gels and then transferred onto an NC membrane (Pall, PAL-66485, NY, USA). Subsequent incubations with corresponding primary and secondary antibodies were conducted. Primary antibodies were diluted according to the manufacturer's instructions. Secondary antibodies used were fluorescence-conjugated (Li-COR Biosciences, 926-68070 and 926-32211, Nebraska, USA) and diluted at 1:20,000. Imaging was acquired using the Li-COR two-color fluorescence imaging system (Li-COR Biosciences, Odyssey CLX, Nebraska, USA) as previously reported (*64*). Primary antibodies were as follows: ATF4 (Cell Signaling Technology, 11815, MA, USA, RRID: AB_2616025), GCN2 (Cell Signaling Technology, 3302, MA, USA, RRID:AB_2277617), p-GCN2 (Abcam, ab75836, Cambridge, UK, RRID:AB_1310260), p-eIF2α (Abcam, ab32157, Cambridge, UK, RRID:AB_732117), eIF2α (Abcam, ab5369, Cambridge, UK, RRID: AB_305008), β-Actin (Proteintech, 66009-1-Ig, Wuhan, China, RRID:AB_2687938), GDF15 (Santa Cruz Biotechnology, sc-515675, CA, USA, RRID: AB_2892674), FGF21 (Abcam, ab171941, Cambridge, UK, RRID: AB_2629460), and UCP1 (Proteintech, 23673-1-AP, Wuhan, China, RRID: AB_2828003).

Real-time qPCR

Total RNA was isolated from tissue samples using the NucleoZol (Gene Co., 740404.200, Nanjing, China) according to the manufacturer's protocol. For Huh-7 cells, RNA-Quick Purification Kit (ESScience, RN001, Shanghai, China) were used according to the manufacturer's protocol. The quantity and purity of RNA were determined using a NanoDrop (Thermo Fisher Scientific, Massachusetts, USA). cDNA was synthesized from 1 μg of total RNA using PrimeScript RT reagent Kit (Takara, RR037A, Kusatsu, Japan) following the manufacturer's instructions. qPCR was performed using the TB Green Premix Ex Taq II (Takara, RR820Q, Kusatsu, Japan) on LightCycler 96 Instrument (Roche, Basel, Switzerland) as previously reported (*65*). Specific primers for target genes (*Atf4*, *Gdf15*, and *Fgf21*) and the reference gene (*Gapdh*) were designed using PrimerQuest Tool of Integrated DNA Technologies (IDT) and Primer-BLAST [National Center for Biotechnology Information (NCBI)]. Primer sequences are available in table S2.

Preparation of RNA-seq samples

In this study, after establishing the HFD-induced obese model in C57BL/6J mice for 12 weeks, the mice were administered with a 100 μg/kg dose of HF or vehicle control via intraperitoneal injection every 2 days for an additional 12 weeks. Subsequently, liver and WAT samples were collected from these mice for transcriptome sequencing as we previously described (*66*). Total RNA was extracted from the tissues using TRIzol reagent (Invitrogen, Carlsbad, CA, USA), following the manufacturer's instructions. RNA quality was assessed using an Agilent 2100 Bioanalyzer (Agilent Technologies, CA, USA) with an RIN value above 7 considered acceptable for RNA-seq. In addition, RNA integrity was verified through ribonuclease-free agarose gel electrophoresis to ensure that the RNA was intact and free from degradation. The total amount of RNA used for sequencing needs to be greater than 1 μg. Ultimately, the qualified liver samples ($n = 5$) and WAT samples ($n = 3$) were used for subsequent transcriptome profiling. RNA preparation, sample quality control, and subsequent data analysis were carried out by Gene Denovo Co. (Guangzhou, China).

Transcriptome sequencing

The resulting cDNA library was sequenced using Illumina Novaseq6000 by Gene Denovo Biotechnology Co. (Guangzhou, China). The experimental workflow primarily encompasses the following steps: (i) transcriptome library construction; (ii) data quality control, which includes filtering low-quality data by removing reads containing adapters, reads with >10% N bases, reads composed entirely of A bases, low-quality reads (where >50% of bases have a quality score $Q \leq 20$), and base quality analysis; (iii) sequence alignment analysis and gene analysis: comprising statistics on gene types, gene coverage, randomness analysis, and saturation analysis; and (iv) expression quantification: Transcripts were reconstructed using StringTie, and the expression levels of all genes in each sample were calculated using RSEM. Expression levels can be presented in two ways: raw reads count and FPKM (fragments per kilobase of transcript per million mapped reads). The data were normalized using FPKM, and hierarchical clustering (Hierarchical Clustering) was used for clustering analysis to visualize gene expression patterns across different samples.

Bioinformatics analysis

On the basis of the gene expression levels, we performed principal components analysis (PCA) using R (version 4.1.2) to investigate the intersample relationships through dimensionality reduction. Correlation analysis between samples was conducted in R using the Pearson

correlation coefficient as a quantitative measure. All data visualization mentioned above was accomplished using R Studio. When conducting PCA, we used the "FactoMineR" (*67*) R package for data processing. The data used were FKPM files obtained through transcriptome sequencing. After data importation, *z*-score normalization was applied, followed by Hierarchical Clustering. For visualizing the PCA results, the "ggplot2" R package was used to differentiate the pca_ result by various groups and overlay elliptical circles. The above data processing process refers to the default parameters described in the "FactoMineR" R package. DESeq2 (*68*) was used for transcriptome differential gene analysis, and genes with a P value <0.01 and $|\log_2 FC| \geq 1.5$ were considered significantly differentially expressed. A volcano plot generated in R was used to visually represent the distribution of differentially expressed genes between comparison groups, while a heatmap presented the hierarchical clustering of differential gene expression patterns. Signaling pathway enrichment analysis for differentially expressed proteins was conducted using the Reactome database (https://reactome.org/).

Accession number

Raw data of RNA-seq were deposited in NCBI Gene Expression Omnibus with accession number GSE273929.

Statistical analyses

Data were expressed as means ± SEM, and the statistical significance was set at $P < 0.05$. The statistical analyses were performed with GraphPad Prism10.0 (GraphPad Software, California, USA) and tested by either Student's *t* test, one-way or two-way analysis of variance (ANOVA) as indicated in the figure legends. The sample size and number of biological replicates for each experiment are described in the figure legends.

Supplementary Materials

This PDF file includes:

Figs. S1 to S9
Tables S1 and S2

REFERENCES AND NOTES

1. C. Hepler, B. J. Weidemann, N. J. Waldeck, B. Marcheva, J. Cedernaes, A. K. Thorne, Y. Kobayashi, R. Nozawa, M. V. Newman, P. Gao, M. Shao, K. M. Ramsey, R. K. Gupta, J. Bass, Time-restricted feeding mitigates obesity through adipocyte thermogenesis. *Science* **378**, 276–284 (2022).
2. A. Sakers, M. K. De Siqueira, P. Seale, C. J. Villanueva, Adipose-tissue plasticity in health and disease. *Cell* **185**, 419–446 (2022).
3. E. E. Calle, C. Rodriguez, K. Walker-Thurmond, M. J. Thun, Overweight, obesity, and mortality from cancer in a prospectively studied cohort of U.S. adults. *N. Engl. J. Med.* **348**, 1625–1638 (2003).
4. A. Afshin, M. H. Forouzanfar, M. B. Reitsma, P. Sur, K. Estep, A. Lee, L. Marczak, A. H. Mokdad, M. Moradi-Lakeh, M. Naghavi, J. S. Salama, T. Vos, K. H. Abate, C. Abbafati, M. B. Ahmed, Z. Al-Aly, A. A. Alkerwi, R. Al-Raddadi, A. T. Amare, A. Amberbir, A. K. Amegah, E. Amini, S. M. Amrock, R. M. Anjana, J. Ärnlöv, H. Asayesh, A. Banerjee, A. Barac, E. Baye, D. A. Bennett, A. S. Beyene, S. Biadgilign, S. Biryukov, E. Bjertness, D. J. Boneya, I. Campos-Nonato, J. J. Carrero, P. Cecilio, K. Cercy, L. G. Ciobanu, L. Cornaby, S. A. Damtew, L. Dandona, R. Dandona, S. D. Dharmaratne, B. B. Duncan, B. Eshrati, A. Esteghamati, V. L. Feigin, J. C. Fernandes, T. Fürst, T. T. Gebrehiwot, A. Gold, P. N. Gona, A. Goto, T. D. Habtewold, K. T. Hadush, N. Hafezi-Nejad, S. I. Hay, M. Horino, F. Islami, R. Kamal, A. Kasaeian, S. V. Katikireddi, A. P. Kengne, C. N. Kesavachandran, Y. S. Khader, Y.-H. Khang, J. Khubchandani, D. Kim, Y. J. Kim, Y. Kinfu, S. Kosen, T. Ku, B. K. Defo, G. A. Kumar, H. J. Larson, M. Leinsalu, X. Liang, S. S. Lim, P. Liu, A. D. Lopez, R. Lozano, A. Majeed, R. Malekzadeh, D. C. Malta, M. Mazidi, C. McAlinden, S. T. McGarvey, D. T. Mengistu, G. A. Mensah, G. B. M. Mensink, H. B. Mezgebe, E. M. Mirrakhimov, U. O. Mueller, J. J. Noubiap, C. M. Obermeyer, F. A. Ogbo, M. O. Owolabi, G. C. Patton, F. Pourmalek, M. Qorbani, A. Rafay, R. K. Rai, C. L. Ranabhat, N. Reinig, S. Safiri, J. A. Salomon, J. R. Sanabria, I. S. Santos, B. Sartorius, M. Sawhney, J. Schmidhuber, A. E. Schutte, M. I. Schmidt, S. G. Sepanlou, M. Shamsizadeh, S. Sheikhbahaei, M.-J. Shin, R. Shiri, I. Shiue, H. S. Roba, D. A. S. Silva, J. I. Silverberg, J. A. Singh, S. Stranges, S. Swaminathan, R. Tabarés-Seisdedos, F. Tadese, B. A. Tedla, B. S. Tegegne, A. S. Terkawi, J. S. Thakur, M. Tonelli, R. Topor-Madry, S. Tyrovolas, K. N. Ukwaja, O. A. Uthman, M. Vaezghasemi, T. Vasankari, V. V. Vlassov, S. E. Vollset, E. Weiderpass, A. Werdecker, J. Wesana, R. Westerman, Y. Yano, N. Yonemoto, G. Yonga, Z. Zaidi, Z. M. Zenebe, B. Zipkin, C. J. L. Murray, Health effects of overweight and obesity in 195 countries over 25 years. *N. Engl. J. Med.* **377**, 13–27 (2017).
5. M. Blüher, Obesity: Global epidemiology and pathogenesis. *Nat. Rev. Endocrinol.* **15**, 288–298 (2019).
6. C. M. Perdomo, R. V. Cohen, P. Sumithran, K. Clément, G. Frühbeck, Contemporary medical, device, and surgical therapies for obesity in adults. *Lancet* **401**, 1116–1130 (2023).
7. T. D. Müller, M. Blüher, M. H. Tschöp, R. D. DiMarchi, Anti-obesity drug discovery: Advances and challenges. *Nat. Rev. Drug Discov.* **21**, 201–223 (2022).
8. M. Davies, L. Færch, O. K. Jeppesen, A. Pakseresht, S. D. Pedersen, L. Perreault, J. Rosenstock, I. Shimomura, A. Viljoen, T. A. Wadden, I. Lingvay, Semaglutide 2·4 mg once a week in adults with overweight or obesity, and type 2 diabetes (STEP 2): A randomised, double-blind, double-dummy, placebo-controlled, phase 3 trial. *Lancet* **397**, 971–984 (2021).
9. P. M. O'Neil, A. L. Birkenfeld, B. McGowan, O. Mosenzon, S. D. Pedersen, S. Wharton, C. G. Carson, C. H. Jepsen, M. Kabisch, J. P. H. Wilding, Efficacy and safety of semaglutide compared with liraglutide and placebo for weight loss in patients with obesity: A randomised, double-blind, placebo and active controlled, dose-ranging, phase 2 trial. *Lancet* **392**, 637–649 (2018).
10. M. Sodhi, R. Rezaeianzadeh, A. Kezouh, M. Etminan, Risk of gastrointestinal adverse events associated with glucagon-like peptide-1 receptor agonists for weight loss. *JAMA* **330**, 1795–1797 (2023).
11. Y. Wu, B. Li, L. Li, S. E. Mitchell, C. L. Green, G. D'Agostino, G. Wang, L. Wang, M. Li, J. Li, C. Niu, Z. Jin, A. Wang, Y. Zheng, A. Douglas, J. R. Speakman, Very-low-protein diets lead to reduced food intake and weight loss, linked to inhibition of hypothalamic mTOR signaling, in mice. *Cell Metab.* **33**, 888–904.e6 (2021).
12. X. Gao, S. M. Sanderson, Z. Dai, M. A. Reid, D. E. Cooper, M. Lu, J. P. Richie, A. Ciccarella, A. Calcagnotto, P. G. Mikhael, S. J. Mentch, J. Liu, G. Ables, D. G. Kirsch, D. S. Hsu, S. N. Nichenametla, J. W. Locasale, Dietary methionine influences therapy in mouse cancer models and alters human metabolism. *Nature* **572**, 397–401 (2019).
13. S. M. Solon-Biet, V. C. Cogger, T. Pulpitel, D. Wahl, X. Clark, E. Bagley, G. C. Gregoriou, A. M. Senior, Q.-P. Wang, A. E. Brandon, R. Perks, J. O'Sullivan, Y. C. Koay, K. Bell-Anderson, M. Kebede, B. Yau, C. Atkinson, G. Svineng, T. Dodgson, J. A. Wali, M. D. W. Piper, P. Juricic, L. Partridge, A. J. Rose, D. Raubenheimer, G. J. Cooney, D. G. Le Couteur, S. J. Simpson, Branched chain amino acids impact health and lifespan indirectly via amino acid balance and appetite control. *Nat. Metab.* **1**, 532–545 (2019).
14. J. Gill, A. Sharma, Prospects of halofuginone as an antiprotozoal drug scaffold. *Drug Discov. Today* **27**, 2586–2592 (2022).
15. T. L. Keller, D. Zocco, M. S. Sundrud, M. Hendrick, M. Edenius, J. Yum, Y.-J. Kim, H.-K. Lee, J. F. Cortese, D. F. Wirth, J. D. Dignam, A. Rao, C.-Y. Yeo, R. Mazitschek, M. Whitman, Halofuginone and other febrifugine derivatives inhibit prolyl-tRNA synthetase. *Nat. Chem. Biol.* **8**, 311–317 (2012).
16. L. Luo, Y. Gao, C. Yang, Z. Shao, X. Wu, S. Li, L. Xiong, C. Chen, Halofuginone attenuates intervertebral discs degeneration by suppressing collagen I production and inactivating TGFβ and NF-κB pathway. *Biomed. Pharmacother.* **101**, 745–753 (2018).
17. J. Wang, B. Wang, X. Lv, Y. Wang, Halofuginone functions as a therapeutic drug for chronic periodontitis in a mouse model. *Int. J. Immunopathol. Pharmacol.* **34**, 2058738420974893 (2020).
18. M. Elkin, I. Ariel, H. Q. Miao, A. Nagler, M. Pines, N. de Groot, A. Hochberg, I. Vlodavsky, Inhibition of bladder carcinoma angiogenesis, stromal support, and tumor growth by halofuginone. *Cancer Res.* **59**, 4111–4118 (1999).
19. M. J. A. de Jonge, H. Dumez, J. Verweij, S. Yarkoni, D. Snyder, D. Lacombe, S. Marréaud, T. Yamaguchi, C. J. A. Punt, A. van Oosterom, Phase I and pharmacokinetic study of halofuginone, an oral quinazolinone derivative in patients with advanced solid tumours. *Eur. J. Cancer* **42**, 1768–1774 (2006).
20. K. P. Stecklair, D. R. Hamburger, M. J. Egorin, R. A. Parise, J. M. Covey, J. L. Eiseman, Pharmacokinetics and tissue distribution of halofuginone (NSC 713205) in CD2F1 mice and Fischer 344 rats. *Cancer Chemother. Pharmacol.* **48**, 375–382 (2001).
21. B. M. Tomazini, L. Tramujas, F. A. Medrado, S. P. D. C. Gomes, K. L. Negrelli, G. S. Murinize, R. H. N. Santos, B. M. P. Vianna, B. F. Piotto, T. S. Veiga, B. R. D. Santos, A. C. P. Horak, O. M. C. Lemos, M. D. A. Lopes, B. B. Olicheski, D. L. Campones, L. A. A. Peixoto, A. D. A. C. Basilio, O. C. E. Gebara, A. T. A. Lopes, H. Saconato, N. Valeis, T. A. Miranda, L. N. Laranjeira, E. V. Santucci, A. F. Carlin, J. D. Esko, P. L. S. M. Gordts, S. Tsimikas, A. B. Cavalcanti, Halofuginone for non-hospitalized adult patients with COVID-19 a multicenter, randomized placebo-controlled phase 2 trial. The HALOS trial. *PLOS ONE* **19**, e0299197 (2024).

22. S. Reagan-Shaw, M. Nihal, N. Ahmad, Dose translation from animal to human studies revisited. *FASEB J.* **22**, 659–661 (2008).
23. M. S. Sundrud, S. B. Koralov, M. Feuerer, D. P. Calado, A. E. Kozhaya, A. Rhule-Smith, R. E. Lefebvre, D. Unutmaz, R. Mazitschek, H. Waldner, M. Whitman, T. Keller, A. Rao, Halofuginone inhibits TH17 cell differentiation by activating the amino acid starvation response. *Science* **324**, 1334–1338 (2009).
24. E. A. Day, R. J. Ford, B. K. Smith, P. Mohammadi-Shemirani, M. R. Morrow, R. M. Gutgesell, R. Lu, A. R. Raphenya, M. Kabiri, A. G. McArthur, N. McInnes, S. Hess, G. Paré, H. C. Gerstein, G. R. Steinberg, Metformin-induced increases in GDF15 are important for suppressing appetite and promoting weight loss. *Nat. Metab.* **1**, 1202–1208 (2019).
25. S.-Y. Zhang, K. Bruce, Z. Danaei, R. J. W. Li, D. R. Barros, R. Kuah, Y.-M. Lim, L. H. Mariani, D. Z. Cherney, J. F. M. Chiu, H. N. Reich, T. K. T. Lam, Metformin triggers a kidney GDF15-dependent area postrema axis to regulate food intake and body weight. *Cell Metab.* **35**, 875–886.e5 (2023).
26. S. Katsumura, N. Siddiqui, M. R. Goldsmith, J. H. Cheah, T. Fujikawa, G. Minegishi, A. Yamagata, Y. Yabuki, K. Kobayashi, M. Shirouzu, T. Inagaki, T. H. M. Huang, N. Musi, I. Topisirovic, O. Larsson, M. Morita, Deadenylase-dependent mRNA decay of GDF15 and FGF21 orchestrates food intake and energy expenditure. *Cell Metab.* **34**, 564–580.e8 (2022).
27. H. Tan, T. Yue, Z. Chen, W. Wu, S. Xu, J. Weng, Targeting FGF21 in cardiovascular and metabolic diseases: from mechanism to medicine. *Int. J. Biol. Sci.* **19**, 66–88 (2023); https://doi.org/10.7150/ijbs.73936.
28. A. P. Coll, M. Chen, P. Taskar, D. Rimmington, S. Patel, J. A. Tadross, I. Cimino, M. Yang, P. Welsh, S. Virtue, D. A. Goldspink, E. L. Miedzybrodzka, A. R. Konopka, R. R. Esponda, J. T. J. Huang, Y. C. L. Tung, S. Rodriguez-Cuenca, R. A. Tomaz, H. P. Harding, A. Melvin, G. S. H. Yeo, D. Preiss, A. Vidal-Puig, L. Vallier, K. S. Nair, N. J. Wareham, D. Ron, F. M. Gribble, F. Reimann, N. Sattar, D. B. Savage, B. B. Allan, S. O'Rahilly, GDF15 mediates the effects of metformin on body weight and energy balance. *Nature* **578**, 444–448 (2020).
29. P. A. Dutchak, T. Katafuchi, A. L. Bookout, J. H. Choi, R. T. Yu, D. J. Mangelsdorf, S. A. Kliewer, Fibroblast growth factor-21 regulates PPARγ activity and the antidiabetic actions of thiazolidinediones. *Cell* **148**, 556–567 (2012).
30. S. Rai, M. Szaruga, A. P. Pitera, A. Bertolotti, Integrated stress response activator halofuginone protects mice from diabetes-like phenotypes. *J. Cell Biol.* **223**, e202405175 (2024).
31. A. P. Pitera, M. Szaruga, S.-Y. Peak-Chew, S. W. Wingett, A. Bertolotti, Cellular responses to halofuginone reveal a vulnerability of the GCN2 branch of the integrated stress response. *EMBO J.* **41**, e109985 (2022).
32. P. Toboz, M. Amiri, N. Tabatabaei, C. R. Dufour, S. H. Kim, C. Fillebeen, C. E. Ayemoba, A. Khoutorsky, M. Nairz, L. Shao, K. V. Pajcini, K.-W. Kim, V. Giguère, R. L. Oliveira, M. Constante, M. M. Santos, C. R. Morales, K. Pantopoulos, N. Sonenberg, S. Pinho, S. Tahmasebi, The amino acid sensor GCN2 controls red blood cell clearance and iron metabolism through regulation of liver macrophages. *Proc. Natl. Acad. Sci. U.S.A.* **119**, e2121251119 (2022).
33. R. Ravindran, J. Loebbermann, H. I. Nakaya, N. Khan, H. Ma, L. Gama, D. K. Machiah, B. Lawson, P. Hakimpour, Y.-C. Wang, S. Li, P. Sharma, R. J. Kaufman, J. Martinez, B. Pulendran, The amino acid sensor GCN2 controls gut inflammation by inhibiting inflammasome activation. *Nature* **531**, 523–527 (2016).
34. S. Liu, J. Yuan, W. Yue, Y. Bi, X. Shen, J. Gao, X. Xu, Z. Lu, GCN2 deficiency protects against high fat diet induced hepatic steatosis and insulin resistance in mice. *Biochim Biophys Acta Mol Basis Dis* **1864**, 3257–3267 (2018).
35. C. Chaveroux, S. Lambert-Langlais, L. Parry, V. Carraro, C. Jousse, A.-C. Maurin, A. Bruhat, G. Marceau, V. Sapin, J. Averous, P. Fafournoux, Identification of GCN2 as new redox regulator for oxidative stress prevention in vivo. *Biochem. Biophys. Res. Commun.* **415**, 120–124 (2011).
36. J. Yuan, Z. Yu, J. Gao, K. Luo, X. Shen, B. Cui, Z. Lu, Inhibition of GCN2 alleviates hepatic steatosis and oxidative stress in obese mice: Involvement of NRF2 regulation. *Redox Biol.* **49**, 102224 (2022).
37. J. Misra, M. J. Holmes, E. T. Mirek, M. Langevin, H.-G. Kim, K. R. Carlson, M. Watford, X. C. Dong, T. G. Anthony, R. C. Wek, Discordant regulation of eIF2 kinase GCN2 and mTORC1 during nutrient stress. *Nucleic Acids Res.* **49**, 5726–5742 (2021).
38. G. J. Wilson, B. A. Lennox, P. She, E. T. Mirek, R. J. T. Al Baghdadi, M. E. Fusakio, J. L. Dixon, G. C. Henderson, R. C. Wek, T. G. Anthony, GCN2 is required to increase fibroblast growth factor 21 and maintain hepatic triglyceride homeostasis during asparaginase treatment. *Am. J. Physiol. Endocrinol. Metab.* **308**, E283–E293 (2015).
39. J. S. Quist, A. B. Klein, K. Færch, K. Beaulieu, M. Rosenkilde, A. S. Gram, A. Sjödin, S. Torekov, B. Stallknecht, C. Clemmensen, M. B. Blond, Effects of acute exercise and exercise training on plasma GDF15 concentrations and associations with appetite and cardiometabolic health in individuals with overweight or obesity - A secondary analysis of a randomized controlled trial. *Appetite* **182**, 106423 (2023).
40. G. Carreras-Badosa, A. Gómez-Vilarrubla, B. Mas-Parés, J.-M. Martínez-Calcerrada, S. Xargay-Torrent, A. Prats-Puig, E. Puerto-Carranza, F. Díaz-Roldán, F. de Zegher, L. Ibañez, J. Bassols, A. López-Bermejo, A 24-month metformin treatment study of children with obesity: Changes in circulating GDF-15 and associations with changes in body weight and visceral fat. *Pediatr. Obes.* **17**, e12845 (2022).
41. A. Sanyal, E. D. Charles, B. A. Neuschwander-Tetri, R. Loomba, S. A. Harrison, M. F. Abdelmalek, E. J. Lawitz, D. Halegoua-DeMarzio, S. Kundu, S. Noviello, Y. Luo, R. Christian, Pegbelfermin (BMS-986036), a PEGylated fibroblast growth factor 21 analogue, in patients with non-alcoholic steatohepatitis: A randomised, double-blind, placebo-controlled, phase 2a trial. *Lancet* **392**, 2705–2717 (2019).
42. D. J. Rader, E. Maratos-Flier, A. Nguyen, D. Hom, M. Ferriere, Y. Li, J. Kompa, M. Martic, M. Hinder, C. T. Basson, D. Yowe, J. Diener, A. B. Goldfine, LLF580, an FGF21 analog, reduces triglycerides and hepatic fat in obese adults with modest hypertriglyceridemia. *J. Clin. Endocrinol. Metab.* **107**, e57–e70 (2022).
43. S. Zheng, D. Polidori, Y. Wang, B. Geist, X. Lin-Schmidt, J. L. Furman, S. Nelson, A. R. Nawrocki, S. A. Hinke, A long-acting GDF15 analog causes robust, sustained weight loss and reduction of food intake in an obese nonhuman primate model. *Clin. Transl. Sci.* **16**, 1431–1444 (2023).
44. X. Guo, P. Asthana, L. Zhai, K. W. Cheng, S. Gurung, J. Huang, J. Wu, Y. Zhang, A. K. Mahato, M. Saarma, M. Ustav, H. Y. Kwan, A. Lyu, K. M. Chan, P. Xu, Z. X. Bian, H. L. X. Wong, Artesunate treats obesity in male mice and non-human primates through GDF15/GFRAL signalling axis. *Nat. Commun.* **15**, 1034 (2024).
45. W. B. Smith, D. Nguyen, T. Clough, J. Schofield, M. R. Kagan, J. Kompa, Y. He, E. Maratos-Flier, J. Jamontt, L. Vong, C. D. Schwartzkopf, J. D. Layne, A. R. Usera, C. J. O'Donnell, K. A. Heldwein, R. S. Streeper, A. B. Goldfine, A growth-differentiation factor 15 receptor agonist in randomized placebo-controlled trials in healthy or obese persons. *J. Clin. Endocrinol. Metab.* **110**, 771–786 (2025).
46. O. Benichou, T. Coskun, M. D. Gonciarz, P. Garhyan, A. C. Adams, Y. Du, J. D. Dunbar, J. A. Martin, K. J. Mather, R. T. Pickard, V. L. Reynolds, D. A. Robins, S. P. Zvada, P. J. Emmerson, Discovery, development, and clinical proof of mechanism of LY3463251, a long-acting GDF15 receptor agonist. *Cell Metab.* **35**, 274–286.e10 (2023).
47. R. Loomba, A. J. Sanyal, K. V. Kowdley, D. L. Bhatt, N. Alkhouri, J. P. Frias, P. Bedossa, S. A. Harrison, D. Lazas, R. Barish, M. D. Gottwald, S. Feng, G. D. Agollah, C. L. Hartsfield, H. Mansbach, M. Margalit, M. F. Abdelmalek, Randomized, controlled trial of the FGF21 analogue pegozafermin in NASH. *N. Engl. J. Med.* **389**, 998–1008 (2023).
48. D. Wang, L. K. Townsend, G. J. DesOrmeaux, S. M. Frangos, B. Batchuluun, L. Dumont, R. E. Kuhre, E. Ahmadi, S. Hu, I. A. Rebalka, J. Gautam, M. J. T. Jabile, C. A. Pileggi, S. Rehal, E. M. Desjardins, E. E. Tsakiridis, J. S. V. Lally, E. S. Juracic, A. R. Tupling, H. C. Gerstein, G. Paré, T. Tsakiridis, M.-E. Harper, T. J. Hawke, J. R. Speakman, D. P. Blondin, G. P. Holloway, S. B. Jørgensen, G. R. Steinberg, GDF15 promotes weight loss by enhancing energy expenditure in muscle. *Nature* **619**, 143–150 (2023).
49. P. J. Emmerson, F. Wang, Y. Du, Q. Liu, R. T. Pickard, M. D. Gonciarz, T. Coskun, M. J. Hamang, D. K. Sindelar, K. K. Ballman, L. A. Foltz, A. Muppidi, J. Alsina-Fernandez, G. C. Barnard, J. X. Tang, X. Liu, X. Mao, R. Siegel, J. H. Sloan, P. J. Mitchell, B. B. Zhang, R. E. Gimeno, B. Shan, X. Wu, The metabolic effects of GDF15 are mediated by the orphan receptor GFRAL. *Nat. Med.* **23**, 1215–1219 (2017).
50. L. Geng, K. S. L. Lam, A. Xu, The therapeutic potential of FGF21 in metabolic diseases: From bench to clinic. *Nat. Rev. Endocrinol.* **16**, 654–667 (2020).
51. C. Cantó, J. Auwerx, Cell biology. FGF21 takes a fat bite. *Science* **336**, 675–676 (2012).
52. Y. Xiong, K. Walker, X. Min, C. Hale, T. Tran, R. Komorowski, J. Yang, J. Davda, N. Nuanmanee, D. Kemp, X. Wang, H. Liu, S. Miller, K. J. Lee, Z. Wang, M. M. Véniant, Long-acting MIC-1/GDF15 molecules to treat obesity: Evidence from mice to monkeys. *Sci. Transl. Med.* **9**, eaan8732 (2017).
53. J. F. Lu, M. Q. Zhu, B. Xia, N. N. Zhang, X. P. Liu, H. Liu, R. X. Zhang, J. Y. Xiao, H. Yang, Y. Q. Zhang, X. M. Li, J. W. Wu, GDF15 is a major determinant of ketogenic diet-induced weight loss. *Cell Metab.* **35**, 2165–2182.e7 (2023).
54. M. Zarei, E. Pujol, T. Quesada-López, F. Villarroya, E. Barroso, S. Vázquez, J. Pizarro-Delgado, X. Palomer, M. Vázquez-Carrera, Oral administration of a new HRI activator as a new strategy to improve high-fat-diet-induced glucose intolerance, hepatic steatosis, and hypertriglyceridaemia through FGF21. *Br. J. Pharmacol.* **176**, 2292–2305 (2019).
55. A. Maida, A. Zota, K. A. Sjøberg, J. Schumacher, T. P. Sijmonsma, A. Pfenninger, M. M. Christensen, T. Gantert, J. Fuhrmeister, U. Rothermel, D. Schmoll, M. Heikenwälder, J. L. Iovanna, K. Stemmer, B. Kiens, S. Herzig, A. J. Rose, A liver stress-endocrine nexus promotes metabolic integrity during dietary protein dilution. *J. Clin. Invest.* **126**, 3263–3278 (2016).
56. K. A. Sjøberg, C. M. Sigvardsen, A. Alvarado-Diaz, N. R. Andersen, M. Larance, R. J. Seeley, P. Schjerling, J. G. Knudsen, G. Katzilieris-Petras, C. Clemmensen, S. B. Jørgensen, K. De Bock, E. A. Richter, GDF15 increases insulin action in the liver and adipose tissue via a β-adrenergic receptor-mediated mechanism. *Cell Metab.* **35**, 1327–1340.e5 (2023).
57. K. Takeuchi, K. Yamaguchi, Y. Takahashi, K. Yano, S. Okishio, H. Ishiba, N. Tochiki, S. Kataoka, H. Fujii, N. Iwai, Y. Seko, A. Umemura, M. Moriguchi, T. Okanoue, Y. Itoh, Hepatocyte-specific GDF15 overexpression improves high-fat diet-induced obesity and hepatic steatosis in mice via hepatic FGF21 induction. *Sci. Rep.* **14**, 23993 (2024).
58. P. Jiang, Z. Liu, T. Fang, Z. Zhang, Y. Zhang, D. Wang, P. J. Little, S. Xu, J. Weng, Growth differentiation factor 15 is dispensable for acetaminophen-induced liver injury in mice. *Basic Clin. Pharmacol. Toxicol.* **132**, 343–353 (2023).

59. Y. Tang, T. Yao, X. Tian, X. Xia, X. Huang, Z. Qin, Z. Shen, L. Zhao, Y. Zhao, B. Diao, Y. Ping, X. Zheng, Y. Xu, H. Chen, T. Qian, T. Ma, B. Zhou, S. Xu, Q. Zhou, Y. Liu, M. Shao, W. Chen, B. Shan, Y. Wu, Hepatic IRE1α-XBP1 signaling promotes GDF15-mediated anorexia and body weight loss in chemotherapy. *J. Exp. Med.* **221**, e20231395 (2024).
60. X. J. Zhang, Z. G. She, J. Wang, D. Sun, L. J. Shen, H. Xiang, X. Cheng, Y. X. Ji, Y. P. Huang, P. L. Li, X. Yang, Y. Cheng, J. P. Ma, H. P. Wang, Y. Hu, F. Hu, S. Tian, H. Tian, P. Zhang, G. N. Zhao, L. Wang, M. L. Hu, Q. Yang, L. H. Zhu, J. Cai, J. Yang, X. Zhang, X. Ma, Q. Xu, R. M. Touyz, P. P. Liu, R. Loomba, Y. Wang, H. Li, Multiple omics study identifies an interspecies conserved driver for nonalcoholic steatohepatitis. *Sci. Transl. Med.* **13**, eabg8117 (2021).
61. S. Chen, X. Liu, C. Peng, C. Tan, H. Sun, H. Liu, Y. Zhang, P. Wu, C. Cui, C. Liu, D. Yang, Z. Li, J. Lu, J. Guan, X. Ke, R. Wang, X. Bo, X. Xu, J. Han, J. Liu, The phytochemical hyperforin triggers thermogenesis in adipose tissue via a Dlat-AMPK signaling axis to curb obesity. *Cell Metab.* **33**, 565–580.e7 (2021).
62. A. I. Mina, R. A. LeClair, K. B. LeClair, D. E. Cohen, L. Lantier, A. S. Banks, CalR: A web-based analysis tool for indirect calorimetry experiments. *Cell Metab.* **28**, 656–666.e1 (2018).
63. S. Xu, X. Wu, S. Wang, M. Xu, T. Fang, X. Ma, M. Chen, J. Fu, J. Guo, S. Tian, T. Tian, X. Cheng, H. Yang, J. Zhou, Z. Wang, Y. Yin, W. Xu, F. Xu, J. Yan, Z. Wang, S. Luo, X.-J. Zhang, Y.-X. Ji, J. Weng, TRIM56 protects against nonalcoholic fatty liver disease by promoting the degradation of fatty acid synthase. *J. Clin. Invest.* **134**, e166149 (2024).
64. S. Xu, Y. Xu, P. Liu, S. Zhang, H. Liu, S. Slavin, S. Kumar, M. Koroleva, J. Luo, X. Wu, A. Rahman, J. Pelisek, H. Jo, S. Si, C. L. Miller, Z. G. Jin, The novel coronary artery disease risk gene JCAD/KIAA1462 promotes endothelial dysfunction and atherosclerosis. *Eur. Heart J.* **40**, 2398–2408 (2019).
65. M. Su, W. Zhao, H. Jiang, Y. Zhao, Z. Liao, Z. Liu, M. Xu, S. Jiang, L. Wu, Y. Yang, Z. Wang, Z. Zeng, Y. Fang, C. Tang, C. L. Miller, P. C. Evans, L. Wang, M. Banach, H. Jo, B. C. Berk, S. Offermanns, Y. Huang, J. Ge, S. Xu, J. Weng, Endothelial IGFBP6 suppresses vascular inflammation and atherosclerosis. *Nat. Cardiovasc. Res.* **4**, 145–162 (2025).
66. M.-Y. Xu, J.-J. Xu, L.-J. Kang, Z.-H. Liu, M.-M. Su, W.-Q. Zhao, Z.-H. Wang, L. Sun, J.-B. Xiao, P. C. Evans, X.-Y. Tian, L. Wang, Y. Huang, X.-M. Liang, J.-P. Weng, S.-W. Xu, Urolithin A promotes atherosclerotic plaque stability by limiting inflammation and hypercholesteremia in Apolipoprotein E-deficient mice. *Acta Pharmacol. Sin.* **45**, 2277–2289 (2024).
67. S. Luo, Y. Chen, X. Su, H. Chu, mmeta: An R package for multivariate meta-analysis. *J. Stat. Softw.* **56**, 11 (2014).
68. M. I. Love, W. Huber, S. Anders, Moderated estimation of fold change and dispersion for RNA-seq data with DESeq2. *Genome Biol.* **15**, 550 (2014).

Acknowledgments: We are grateful to J. Liu and X. Zhang (Hefei University of Technology); J. Wu (Soochow University); Z. Yin (Jinan University), C. Zhan, and Y. Duan (University of Science and Technology of China); and Z. Zheng (Medical College of Wisconsin, Milwaukee, USA) for insightful discussions. We also thank Z. Xie (Anhui Agricultural University) and Y. Chen (Hefei University of Technology) for assistance in body composition assay. We thank the members of the Weng laboratory for valuable discussions and feedback. **Funding:** This study was supported by grants from the National Key R&D Program of China (grant no. 2021YFC2500501, to J.W.) and the National Natural Science Foundation of China (grant nos. 82370444, 82070464, and 12411530127, to S.X.). This work was also supported by the Program for Innovative Research Team of The First Affiliated Hospital of USTC (CXGG02, to J.W.), Anhui Provincial Natural Science Foundation (grant no. 2208085 J08, to S.X.), USTC Research Funds of the Double First-Class Initiative (no. YD9110002089, to S.X.), and the Research Funds of Centre for Leading Medicine and Advanced Technologies of IHM (to S.X.). **Author contributions:** Conceptualization: Z.L., S.X., D.W., P.J.L., J.R.S., Z.W., and J.W. Methodology: Z.L., S.X., J.R.S., M.-d.L., W.Z., F.Z., and S.O. Software: D.W., T.T., and Z.W. Validation: Z.L., T.T., S.X., W.Z., M.L., Z.W., and M.S. Formal analysis: Z.L., T.T., M.-d.L., J.R.S., S.X., Z.W., and J.W. Investigation: W.P., Z.L., S.L., W.F., M.C., M.X., T.T., W.Z., Z.Z., S.X., and M.L. Resources: W.P., S.L., S.O., Y.Y., P.J.L., S.X., M.S., and J.W. Data curation: Z.L., W.F., W.Z., J.R.S., S.X., Z.W., and J.W. Writing—original draft: Z.L., Y.Y., T.T., J.R.S., S.X., Z.W., and J.W. Writing—review and editing: W.P., Z.L., S.O., P.J.L., T.T., M.-d.L., W.Z., J.R.S., S.X., Z.W., S.Z., D.W., D.K., and J.W. Visualization: Z.L., P.J.L., Z.Z., S.X., Z.W., and J.W. Supervision: J.R.S., S.X., and J.W. Project administration: W.P., S.X., and J.W. Funding acquisition: S.X. and J.W. **Competing interests:** J.W. and S.X. are inventors on a patent 202210110323 filed by University of Science and Technology of China on the use of halofuginone in treating obesity (filed on 29 January 2022; granted on 21 April 2023). S.X. is Senior Humboldt Research Fellow of Alexander von Humboldt Foundation, Germany. All other authors declare that they have no competing interests. **Data and materials availability:** All data needed to evaluate the conclusions in the paper are present in the paper or/and the Supplementary Materials. Raw data of RNA-seq were deposited in Gene Expression Omnibus with accession number: GSE273929.

Submitted 22 September 2024
Accepted 20 February 2025
Published 26 March 2025
10.1126/sciadv.adt3142